

THESIS

MORPHODYNAMIC MODELING OF FLOW AND SEDIMENT TRANSPORT OVER
LOW-HEAD, RUN-OF-RIVER DAMS

Submitted by

Robert William Queen

Department of Civil and Environmental Engineering

In partial fulfillment of the requirements

For the Degree of Master of Science

Colorado State University

Fort Collins, Colorado

Summer 2018

Master's Committee:

Advisor: Peter A. Nelson

Ryan R. Morrison

Sara L. Rathburn

Copyright by Robert William Queen

All Rights Reserved

ABSTRACT

MORPHODYNAMIC MODELING OF FLOW AND SEDIMENT TRANSPORT OVER LOW-HEAD, RUN-OF-RIVER DAMS

Low-head or Run-of-River (RoR) dams exist on all types of rivers throughout the United States, yet the exact mechanisms of how sediment moves around the structures have not been well researched. Due to the increasing use of RoR dams in small hydroelectric projects, there is a need to better understand the controlling factors of how sediment passes over these dams. A one-dimensional morphodynamic model was developed to investigate the effects of RoR dams on channel morphology over long time scales. The model solves the gradually varied flow equations to compute the flow field in the vicinity of the dam, computes grain-size-specific sediment transport rates, and uses sediment mass conservation and vertical storage bookkeeping to calculate the evolution of bed elevation, the bed surface grain-size distribution, and the vertical pattern of stratigraphy. The model's hydraulic calculations were calibrated using data collected from a series of flume experiments performed with a model RoR dam to better capture the non-hydrostatic flow over a dam. Numerical experiments designed to investigate how the grain-size distribution of the sediment supply rate, flow rate (steady and unsteady), and dam height act as controls on sediment passage over RoR dams were conducted using parameters reported in the literature for a RoR dam in northern Delaware. These one-dimensional simulations were complemented with a few simulations using a two-dimensional morphodynamic model, Nays2DH. The 1D simulation results show that the stored sediment upstream of RoR dams does depend on the sediment supply, dam height, grain-size and flow discharge. Once sedimentation in the reservoir has reached equilibrium, high flow events will reduce or scour the sediment while lower flows will typically increase the amount of sediment behind the dam. Finally, a dam that stores more sediment will have greater downstream effects in terms of changes to grain-sizes and bed elevation due to the increased time it

takes to pass sediment over the dam and reach an equilibrium condition on the upstream side of the dam.

ACKNOWLEDGEMENTS

I would like to thank the Hydro Research Foundation for financial support of my thesis. The Hydro Research foundations seeks to facilitate research and educational opportunities as well as promote the value of hydropower in our society as a beneficial source of energy. This support allowed me to pursue this research on Run-of-River dams as part of my master's program. The Hydro Research Foundation funds are possible through a grant by the United State Department of Energy. A big thanks to Dr. Peter Nelson for providing invaluable advice and guidance throughout both my research and writing. Also, thank you to my committee members, Dr. Sara Rathburn and Dr. Ryan Morrison for their help. Thanks to Jacob Morgan for helping me to learn Fortran and for the use of the initial model code. Lastly, I would like to thank Colorado State University and the Engineering Research Center for the use of computing resources and the laboratory space for my flume experiment.

TABLE OF CONTENTS

ABSTRACT	ii
ACKNOWLEDGEMENTS	iv
LIST OF TABLES	vii
LIST OF FIGURES	viii
Chapter 1 Introduction	1
Chapter 2 Methods	5
2.1 Experimental Observations of Flow over ‘RoR’ Dams	5
2.2 One Dimensional Morphodynamic Model	6
2.2.1 Hydraulic Calculations	7
2.2.2 Sediment Transport Calculations	11
2.2.3 Bed Evolution	14
2.2.4 Model Calibration	18
2.2.5 iRIC Interface Connection	18
2.3 One Dimensional Morphodynamic Model Runs	18
2.4 Two Dimensional Morphodynamic Model Runs	22
Chapter 3 Results	23
3.1 Flume Experiment Results	23
3.1.1 Water Surface Measurements	23
3.1.2 Velocity Measurements	24
3.2 One Dimensional Morphodynamic Results	26
3.2.1 Flume Calibration Results	26
3.2.2 Model Runs	27
3.2.3 Comparison to models with no dam	39
3.3 Two Dimensional Morphodynamic Results	40
Chapter 4 Discussion	42
4.1 Flume Experiment Implications	42
4.2 Controls on Sediment Storage in RoR Dam Reservoirs	45
4.3 Scouring of Sediment During High Flows	46
4.4 Downstream and Upstream Effects	49
4.5 Two Dimensional Model	51
Chapter 5 Conclusion	53
Appendix A iRIC Interface Guide	60
A.1 Introduction	60
A.2 Guide	60
A.3 Conclusion	63
A.4 Attached Files	63

Appendix B Suspended Sediment Transport 64

LIST OF TABLES

2.1 Summary of 1D Model Runs	19
----------------------------------------	----

LIST OF FIGURES

2.1	Flume Experiment View	5
2.2	Summary of grain-size Distribution	21
3.1	Picture of Flow in Flume Experiment	24
3.2	Water Surface Elevations for Flume Experiment	25
3.3	Detailed Velocity Profile for Flume Experiment	26
3.4	1D Model Validation with Flume Experiment	27
3.5	Statigraphy at 45 Days for Base Model	28
3.6	Stored Sediment for Changes in Upstream Sediment Supply	29
3.7	Changes in Bed Elevation and grain-size Upstream of Dam	30
3.8	Changes in Bed Elevation and grain-size Downstream of Dam	31
3.9	Stored Sediment for Changes in grain-size - Equilibrium Condition	32
3.10	Stored Sediment for Changes in grain-size - Steady Supply Rate	32
3.11	Stored Sediment for Changes in Dam Heights	33
3.12	Stored Sediment for Changes in Steady Discharge	34
3.13	Maximum Sediment Above Dam for Various Control Parameters	34
3.14	Stored sediment for Unsteady Flow	36
3.15	Stored Sediment for Unsteady Flow with Flow Rate	37
3.16	Stored Sediment for Unsteady Flow with Limited Sediment	38
3.17	Change is Stored Sediment Versus the Flow Rate	38
3.18	Changes in Bed Elevation and Median grain-size with Increasing Flow	39
3.19	Changes over Time for Bed Elevation and Mean Grain Diamter for 2D Model	41
4.1	Shields Parameter and Bedload Transport Rate for Changes in Steady Discharge	47

Chapter 1

Introduction

Throughout the United States, there are thousands of low-head or Run-of-River (RoR) dams in use for diversion structures and hydroelectric power. In the past (starting in the mid 19th century and continuing on to the early 20th century), many of these small dams were built in the north-eastern portion of the United States for use in mills and agricultural purposes. As the settlers of the United States expanded into the western region of the US, many small dams were placed in rivers as a way to divert water for irrigation and municipal water supply (*Csiki and Rhoads, 2010*). In recent years, RoR dams have been increasingly used in small hydropower projects as a way to increase the grid reliability and the renewable energy portfolio (*Fuller et al., 2016*). In 2013, President Obama signed the "Hydropower Regulatory Efficiency Act of 2013" which sought to promote the development of smaller hydropower projects by decreasing regulations and streamlining the permitting (*Jayjack, 2018*). As a result of this change, as well as tax credits and public desire for more environmentally friendly electric power, the use of these RoR dams for small hydropower has been increasing in recent years (*Warren, 2014*).

Due to the small size of these dams, they are often considered inconsequential in terms of the effects on sediment transport and the resulting impact on river morphology. However, this question has not been well studied on rivers with smaller dams (*Csiki and Rhoads, 2010*). To evaluate the effects of small RoR dams on sediment transport and river morphology requires taking the research and assumptions from large scale effects of dams (*Williams and Wolman, 1985*) and applying them to these much smaller RoR dams. For a large scale dam, the lack of downstream sediment supply due to sedimentation behind the dam causes the bed downstream of the dam to degrade in elevation and increase the median grain diameter of the bed material (*Pizzuto, 2002; Williams and Wolman, 1985*). In terms of other impacts of dams, the impact of river morphology from dams has been well studied in the literature (*Csiki and Rhoads, 2010; Fuller et al., 2016; Pearson and Pizzuto, 2015; Pizzuto, 2002; Williams and Wolman, 1985*) especially as related to more traditional larger

dams. In large dams, reservoir sedimentation may produce a delta that leads into the foreset at the head of the reservoir on the upstream section of the dam. The delta stratigraphy consists of coarser sediment settles on the top of the delta as the water slows and the shear velocity decreases in the the backwater area caused by the dam. Finer sediment is able to travel further and the bedload rests to create the foreset which is the transition between the original bed and that of the delta region being built up due to the deposition of sediment (*Lajczak, 1996*). The suspended sediment and wash load concentration may be transported further downstream into the deeper parts of the reservoir which might cause fine sediment to be deposited closer to the dam depending on the specific concentrations present in the flow (*Csiki and Rhoads, 2010*).

Much of the research focused on RoR dams has been spent on field investigations of existing RoR dams (*Anderson et al., 2015; Csiki and Rhoads, 2014; Pearson and Pizzuto, 2015; Sindelar et al., 2017*) and the impacts they have on the river. *Csiki and Rhoads (2014)* found that these dams produced minimal changes to the river upstream and downstream of the dam. These RoR dams were situated on flat reaches in Illinois with little sediment supply which might not make them translate well to gravel bed reaches where RoR systems are often placed. RoR dams that produce hydropower tend to be situated on gravel bed streams as gravel bed streams primarily exist in mountainous regions with large enough hydraulic heads to make the construction of RoR dams economically viable (*Fuller et al., 2016*). *Csiki and Rhoads (2014)* noted that the hydraulics upstream of the dam have not been well studied and the authors speculated that the turbulence and diminishing value of the backwater behind the dam at high flows caused sediment to scour out from above the dam. *Pearson and Pizzuto (2015)* suggested that high flow periods contributed to scouring of sediment over the dam but did not have direct field or other observations to confirm this claim. In addition, that study suggests a sediment ramp mechanism where sediment aggrades upstream of the dam in the form of a ramp which helps facilitate sediment transport over the dam. Due to the increasing nature of dam removals especially on RoR dams, many of the other studies specifically look at scouring during dam removals or on RoR dams with weirs that open. This research only focuses on permanent RoR dams without weirs that open but these studies can help

to further understand how sediment moves during periods of higher flow. *Pizzuto* (2002) provides insight into the geomorphic processes during a dam removal including incision of flow into the stored sediment behind the dam and how the trapped sediment that remained behind the dam moves through the reach after the dam is gone especially as relating to the removal of smaller, low-head dams. This degradation provides insight to possible mechanisms of scouring out sediment during high flows and how this process occurs.

There remains a large knowledge gap regarding the effects on these dams on the hydraulics, sedimentation, and upstream and downstream morphology (*Csiki and Rhoads*, 2010). The main goal of this research is to better understand the nature of flow, sediment transport and sediment deposition over and around RoR dams and their effects on the geomorphology of the river upstream and downstream of the dam. This could in turn have implications to aquatic habitat and other environmental considerations around these dams.

Overall, this paper and research is focused on addressing three hypotheses related to RoR dams:

1. The amount of sediment stored above a RoR dam will depend on the upstream sediment supply, dam height, grain-size, and discharge.
2. The amount of sediment stored above RoR dams will dynamically shift under unsteady flow conditions, scouring at high flow and filling at low flow.
3. The upstream and downstream effects of RoR dams will depend upon the sediment storage efficacy of the dam. Dams that store more sediment will have a greater effect upstream and downstream than dams that store less sediment.

I use a morphodynamic model to investigate the above hypotheses. Morphodynamic models have proved useful to better understand how rivers respond to various management and restoration activities on the river (*McDonald et al.*, 2010). These models allow important parameters such as the flow rate, dam height, grain-size distribution, sediment supply rate, and channel width to be varied. The one-dimensional model used here was originally developed by Jacob Morgan of Colorado State University for the investigation of riffle-pool dynamics in variable width channels

(*Morgan and Nelson, 2016*). Here I have modified the model to work especially for RoR dams and accept a wider range of functions and inputs such as varying flow data and geometric data.

To verify the model's computations of hydraulics of flow over a RoR dam, a flume experiment was performed to document the flow structure over a RoR dam at different discharges and to provide validation data for the model that helped to modify hydraulic calculations. In terms of hydraulic impact of RoR dams, the research has focused on avoiding the dangerous condition for boaters and swimmers that travel over RoR dams in the design of these dams (*Leutheusser and Birk, 1991; Leutheusser and Fan, 2001*). However, only minimal work has been done as a way to apply this work to a one-dimensional numerical model (*Castro-Orgaz, 2010*).

The one-dimensional model uses the standard-step method (*Chow, 1959*) to compute the hydraulics. The standard-step method relies on the assumption of gradually-varied flow where the velocity or depth do not rapidly change, meaning that the pressure can be approximated as hydrostatic. However, even small RoR dams cause the flow to become rapidly-varied and non-hydrostatic (*Strum, 2010*). The flow takes a curvilinear flow path based on the geometry parameters of the dam (*Castro-Orgaz, 2010; Hager, 2010*). Based on these flow conditions, it is not easy to accurately model the conditions around a dam or obstruction in a standard one-dimensional model. I therefore performed a flume experiment to gain a more complete understanding of the complex hydraulics of flow over a RoR dam, and I used these observations to modify the hydraulic calculations of the one-dimensional model to make it more applicable to RoR conditions.

The 1D model, the flume observations, and the 2D model are used to explore the three hypotheses listed above and to better understand run-of-river dams and their impact on river morphology and dynamics.

Chapter 2

Methods

2.1 Experimental Observations of Flow over ‘RoR’ Dams

The flume experiment was conducted at the Engineering Research Center of Colorado State University in an 8.5-inch-wide (21.7 cm), 30-foot (9.1 m) long, 3-foot (0.91 m) deep, rectangular plexiglass flume as a way to better characterize the hydraulics around RoR dams. The flume slope was set to 1.18% (the device to set the slope did not allow me to set it to a more round number such as 1%), which is typical of gravel bed rivers where RoR dams are often present (Pearson and Pizzuto, 2015; Sindelar et al., 2017). A four-inch (10.2 cm) tall dam made of wood was glued to the bed in the middle of the flume. The dam had sloping walls of 72.5° which matched data in RoR dams col-



Figure 2.1: View of flume experiment with dam in the middle of the flume

lected and described by Csiki and Rhoads (2014). The bottom length was 4.0 inches and the top length was 2.0 inches (5.1 cm). A view of the dam in the flume is seen in Figure 2.1. Four different flume experiments (A, B, C, and D) were conducted at 0.042 cfs (0.00119 cms), 0.158 cfs (0.00447 cms), 0.219 cfs (0.00620 cms) and 0.540 cfs (0.0153 cms).

For each of these discharges (Experiments A, B, C, D), the following tests were done (referred to as runs). Run 1 was the condition with no backwater effects downstream. Run 2 was the condition of a hydraulic jump near the dam. Run 3 was where the jump was submerged and in the

condition of a dangerous weir or deadly weir with circular flow patterns. Run 4 was a bit more submerged than the conditions in Run 3. These tests varied a bit because it was hard to control the downstream sluice gate accurately and slight adjustments to the gate could cause delayed and large changes in the downstream condition. These tests were developed as shown in the various cases of low head dams in *Leutheusser and Birk* (1991). Using a Nortek Acoustic Doppler Velocimeter measurement (ADV) (*Lohrmann et al.*, 1994; *Nikora and Goring*, 1998; *Nortek*, 2015), a detailed set of velocity measurements was taken from upstream of the dam to about halfway to the upstream end of the flume. Velocity measurements were collected 0.2, 0.6 and 0.8 times the depth of flow at four points in the cross sections with two locations in the center and the others closer to the side of the channel. Each velocity measurement was collected at a 200 Hz sampling rate over approximately 30-60 seconds. In each test a velocity profile in the center of the channel was taken just upstream of the dam, over the dam (if possible) and just downstream of the dam only in the center of the channel. These profiles were taken at 0.5 cm to 1.5 cm increments depending on the depth of flow to get around 10 total measurements over the depth and possibly many more. If the flow conditions did not have a significant change meaning that the depth of flow did not change from one run to the other, no additional measurement was taken for that test. In addition, the water surface profile in the area around the dam was recorded using a ruler. These water surface elevations were taken at 1 cm (0.39 in) intervals for at least 10 cm (3.9 in) on either side of the dam.

Velocity data were averaged in the downstream (x), cross stream (y) and vertical (z) directions and fluctuations from the average were used to calculate turbulence characteristics. The *Goring and Nikora* (2002) despiking algorithm was considered, but it was determined not to be necessary for the vast majority of the collected data.

2.2 One Dimensional Morphodynamic Model

I used a one-dimensional morphodynamic model that calculates the cross-sectionally averaged hydraulics, sediment transport, and the bed evolution while storing stratigraphy of the bed material

for periods of aggradation and degradation. The model follows the work done both in *Morgan and Nelson (2016)* and *Viparelli et al. (2010a)* with modifications for the application to RoR dams. The model was written in Fortran 90 because this allowed for much faster computations than possible in scripting languages such as Matlab and allowed for easier connection to the iRIC interface (*Nelson et al., 2016*).

2.2.1 Hydraulic Calculations

The model calculates hydraulics following the standard step method for one-dimensional flow that has extensive use in many hydraulic models (*Chow, 1959; Henderson, 1966*). Flow is initially calculated assuming a subcritical flow and starts downstream from a given boundary condition which in this case is normal depth at the downstream end. It assumes the same depth at the next upstream node as a trial value. Next, various trial parameters are calculated that include the mean flow velocity (u), the velocity head, the Froude number (Fr), the total energy head and the hydraulic radius (R_h). The flow resistance is based on a friction coefficient, C_f assuming that the total shear stress derives from the grain shear alone. The friction coefficient is then related to the total shear stress, τ by:

$$\tau = \rho C_f u^2 \quad (2.1)$$

where ρ is the density of water. Using the Manning-Strickler relations based on *Parker (1991, 2006)* one can relate the friction coefficient to the roughness height that compares well to the Law of the Wall relation:

$$C_f^{-1/2} = \frac{u}{u_*} = 8.1 \left(\frac{R_h}{k_s} \right)^{1/6} \quad (2.2)$$

where u_* is the shear velocity where $u_* = \sqrt{\tau/\rho}$ and k_s is the roughness height where $k_s = n_k d_{90}$ in which n_k is a constant taken as 2 for the model run but can be changed in the code and d_{90} is the sediment size for which 90 percent is finer.

Another relationship for the shear stress is based on the friction slope, S_f as given by:

$$\tau = \gamma R_h S_f \quad (2.3)$$

where $\gamma = \rho g$ such that g is the acceleration due to gravity. Combining the two shear stress relationships and solving for the friction slope gives an expression that can be used to find the friction slope based on the Manning-Strickler relationship.

$$S_f = C_f \frac{u^2}{gR_h} \quad (2.4)$$

Once this trial friction slope is known, one can find the average friction slope between the nodes, \bar{S}_f , which in this program is computed using a simple arithmetic average. From this, the expected head loss, h_f for the friction slope over the length, δx is found based on:

$$h_f = \bar{S}_f \Delta x \quad (2.5)$$

From this, the total energy, E at the downstream node is known and the trial total energy at the current node is known as well as the expected energy loss between them. The trial total energy plus the head loss should equal the downstream energy. The total energy is given by:

$$E = \eta + h + h_v \quad (2.6)$$

where η is the bed elevation, h is the flow depth and h_v is the velocity head where $h_v = u^2/(2g)$.

Often, the trial value of depth is incorrect, so a new value of depth needs to be chosen. For this adjustment, a Newton-Raphson convergence method is used (*Henderson, 1966*). This method produces a correction value which is then subtracted from the trial depth to produce a new depth in which the above calculations are repeated until the difference in total energies and head loss is within a tolerance value specified in the program. Sometimes this does not converge, especially if the flow is actually supercritical, which in this case the depth is set temporarily to the critical depth.

Once the subcritical calculations are complete, the program completes the supercritical calculations along the entire reach starting from the upstream end. The upstream boundary condition is

set to the critical depth. It then goes through the same calculations as before in the downstream direction until it reaches the end of the reach. If the program cannot converge, the depth is set to 1.05 times the critical depth value.

After the supercritical calculations are complete, the two depths (those found during the supercritical and subcritical computations, respectively) are compared using the momentum function, M at each cross section (*Strum, 2010*). For a rectangular cross section, the momentum function is given by:

$$M = \frac{Q^2}{BHg} + 0.5H^2B \quad (2.7)$$

The depth with the largest momentum at each cross section is the state of the flow at each node. This method can capture hydraulic jumps and transitions of state of flows. Finally, all flow parameters are recalculated for the reach based on the determined values. This includes the flow velocity, the velocity head, the Froude number, the total energy, the flow resistance, the friction slope and the Shields stress. The Shields stress, τ_{*g} given by:

$$\tau_{*g} = \frac{\tau}{R\gamma d_g} = \frac{C_f u^2}{Rg d_g} \quad (2.8)$$

where R is the submerged specific gravity of the sediment and d_g is the geometric mean grain-size of the bed sediment. After this, it makes some checks to determine there were no errors in the calculations and then ends the hydraulic calculations. Using the determined hydraulic calculation values, the program moves on to the bedload and suspended sediment calculations.

Non-Hydrostatic Computation Correction

The flow over the dam cannot be accurately computed by the above methods, which assume gradually varied flow and flow that has a hydrostatic pressure distribution (*Chow, 1959; Strum, 2010*). The flow over the dam becomes rapidly varied, meaning the flow does not have a hydrostatic pressure distribution, and this causes curvature of flow over the dam. To help account for this, a correction factor is added in the computation of the total energy at locations around the dam. This result provides an approximation of non-hydrostatic flow, although to fully resolve this

issue, one would need a multi-dimensional hydraulic model which would remove the hydrostatic assumption.

To compute the non-hydrostatic correction, I adopt a method presented by *Hager* (2010) in response to *Castro-Organ* (2010). This method calculates a parameter Ω using the differences in the changes of the angle, θ of the bed slope given by:

$$\Omega = \exp(\kappa N_h) \quad (2.9)$$

where N_h is the vertical depth where $h \approx N_h \cos \theta$ (this involves a simplification and removes higher order terms) and $\kappa \approx \partial\theta/\partial x$ which captures the curvature of the bottom profile. The computation of the θ is found by the inverse tangent of the bed slope.

To improve accuracy of the partial differential, a three point central difference was used where:

$$\frac{\partial\theta}{\partial x} \approx \left(-\frac{1}{60}\theta_{i-3} + \frac{3}{20}\theta_{i-2} - \frac{3}{4}\theta_{i-1} + \frac{3}{4}\theta_{i+1} - \frac{3}{20}\theta_{i+2} + \frac{1}{60}\theta_{i+3} \right) / \Delta x \quad (2.10)$$

where the subscript, i represents the current node. From this, a value of Ω can be computed using the above equation. If the value of Ω is less than 0.3679 it is set at 0.3679 and if it is greater than 1.6487 it is set at 1.6487. This helps prevent calculation of extreme values and avoids sudden large changes in the water surface elevation. From this a new upstream energy can be computed by:

$$E = \eta + N_h \cos \theta + \frac{q^2}{2gN_h^2} \Omega \quad (2.11)$$

Note how in a flat bed with no curvature, Ω goes to one which makes no change to the energy head. This addition to the hydraulic computations around the dam allows them to better capture the curvature of the flow as seen in the flume experiments. This means that in locations around the dam, the energy is computed using the a modified depth with a factor applied to the velocity head.

2.2.2 Sediment Transport Calculations

After the hydraulic results have been completed, the program goes into the computations of the sediment transport calculations. The program two options for bedload transport computations: a modified version of the Ashida-Mishue (1972) relation based on an update by *Viparelli et al.* (2010b), or the relation developed in *Wilcock and Crowe* (2003). Both relations use information from the hydraulics and output the unit bedload discharge as well as the grain-size distribution of the bedload at each spatial node.

In addition, a suspended sediment model has been implemented in my model using the methods of *Garcia and Parker* (1991); *Parker* (1991); however, in this paper I only simulate bedload transport. See Appendix B for details about the suspended sediment model.

Ashida-Mishue Bedload Relationship

The Ashida and Michue (1972) bedload relation was developed original for sand and pea sized gravel. My model implements the *Viparelli et al.* (2010b) modification to the hiding function based on their flume experiment.

The code calculates the bedload at each spatial node. For each i th fraction of the grain-size distribution, it first calculates a parameter, $n_p = d_i/d_g$ where d_i is the grain-size at the current node and d_g is the geometric mean grain-size. From this, it calculates the critical Shields parameter for each grain-size range, τ_{ci}^* .

$$\tau_{ci}^* = \begin{cases} \tau_{ref}^* n_p^{-0.68} & n_p > 1 \\ \tau_{ref}^* n_p^{-0.98} & n_p \leq 1 \end{cases} \quad (2.12)$$

where τ_{ref}^* is the reference Shields stress and set as 0.043 based on the data used in the paper. Next, the effective shear stress for each grain-size, τ_{bi}^* is found based on the following relation.

$$\tau_{bi}^* = \frac{\tau^*}{n_p} \quad (2.13)$$

where τ^* is the Shields stress from the hydraulic computations. If $\tau_{bi}^* < \tau_{ci}^*$ then the volumetric bedload rate per unit width for that grain-size, q_{bi} is set as zero. Otherwise, the bedload rate is determined by:

$$q_{bi} = 17\alpha (\tau_{bi}^* - \tau_{ci}^*) \left(\sqrt{\tau_{bi}^*} - \sqrt{\tau_{ci}^*} \right) \sqrt{Rgd_i} d_i F_i \quad (2.14)$$

where, R is the submerged specific gravity of the sediment which is set at 1.65, α is a correction factor set at 0.27 and F_i is the fraction of each grain-size in the bed material. The total unit bedload rate is then computed as the sum of all the bedload rates for each grain-size.

Wilcock-Crowe Bedload Relationship

The Wilcock and Crowe (*Wilcock and Crowe, 2003*) surface-based transport model for mixed size sediment is a commonly used transport model for mixed sand and gravel sized sediments. This model may be appropriate in my application as many RoR dams exist on gravel bed rivers (*Csiki and Rhoads, 2010; Pearson and Pizzuto, 2015*). Like many other models, the equation implements a hiding function to compute lower transport of smaller grain-sized particles.

At each node in the spatial direction, this formulation is computed. First, the sand fraction percent of the surface grain-size is computed based on the percentage of particles less than 2 mm in the partial distribution. From the hydraulic calculations, the Shields parameter has already been computed and from this, the shear stress is calculated using:

$$\tau = \tau_* R \rho g d_g \quad (2.15)$$

where τ is the shear stress, τ_* is the Shields stress, R is the submerged specific sediment gravity, and d_g is the mean grain diameter of the surface sediment. Then the shear velocity, u_* is calculated:

$$u_* = \left(\frac{\tau}{\rho} \right)^{0.5} \quad (2.16)$$

Next, the reference Shields shear stress, τ_{rm}^* is calculated based on the percent sand on the bed surface, F_s that was previously found.

$$\tau_{rm}^* = 0.021 + 0.015 \exp(-20F_s) \quad (2.17)$$

From this, the reference shear stress, τ_{rm} is calculated.

$$\tau_{rm} = \tau_{rm}^* R \rho g d_g \quad (2.18)$$

The model then loops through each grain-size in relation to the partial distribution for each node. A parameter, b is first calculated which will be used as an exponent for the hiding function relation.

$$b = \frac{0.67}{1 + \exp\left(\frac{D_i}{D_g}\right)} \quad (2.19)$$

where D_i is the grain-size in the partial distribution. Then, the reference shear stress, τ_{ri} is computed using:

$$\tau_{ri} = \tau_{rm} \left(\frac{D_i}{D_g}\right)^b \quad (2.20)$$

Next, a value, ϕ is set where $\phi = \tau/\tau_{ri}$. From this value, the dimensionless transport rate of size fraction i , W_i^* is computed using:

$$W_i^* = \begin{cases} 0.002\phi^{7.5} & \phi < 1.35 \\ 14 \left(1 - \frac{0.894}{\phi^{0.5}}\right)^{4.5} & \phi \geq 1.35 \end{cases} \quad (2.21)$$

From this, the volumetric transport rate per unit width of each size fraction i , q_{bi} , is computed using:

$$q_{bi} = \frac{W_i^* u_*^3 F_i}{Rg} \quad (2.22)$$

where F_i is the fraction of each grain-size in the bed material. The total load is then found by summing up all the load of each fractional grain-size. The grain-size distribution of the bedload material is found by taking the fractional transport rate over the total transport rate. This process is then repeated for each node along the reach.

2.2.3 Bed Evolution

Once the program computes the bedload and suspended sediment load at each node, it can then compute the changes in the bed elevation and grain-size. To do this, the sediment continuity equation (also called the Exner Equation) is used. The process is described below based on both bedload and the suspended sediment load.

Exner Equation - Combined Sediment Load with Fractional grain-sizes

The one-dimensional Exner equation for bed load and suspended sediment load with fractional grain-sizes is presented below. It is in two forms as one looks at the change in bed elevation and the other looks at the change in the fractional content of the bed material. The second equation is for aggradation only and is not used for degradation. This assumes constant width and ignores subsidence and effects of floods. The derivation of these equations comes from conservation of sediment mass and is not presented here. The i notation is for each grain-size in the sediment mixture distribution. The j notation is for each spatial node in the stream-wise direction along the reach from upstream to downstream. The k notation is current time.

$$\frac{\partial \eta}{\partial t} = -\frac{1}{1 - \lambda_p} \frac{\partial (q_{bT} + q_{sT})}{\partial x} \quad (2.23)$$

$$L_a \frac{\partial F_i}{\partial t} = -\frac{1}{1 - \lambda_p} \left[\frac{\partial (q_{bi} + q_{si})}{\partial x} - f_{li} \frac{(q_{bT} + q_{sT})}{\partial x} \right] \quad (2.24)$$

where η is the bed elevation, t is the time, λ_p is the porosity of the sediment (around 0.4), q_{bT} is the total bed load transport, q_{sT} is the total suspended load transport (see Appendix B), q_{bi} is the fractional bed load transport, q_{si} is the fractional suspended load transport, x is the distance, L_a is the active layer thickness, F_i is the fraction of sediment in each size range in the active layer, and f_{li} is the fraction of sediment in each size range deposited to the substrate, composed of a fraction α of bed material and $(1 - \alpha)$ of load material:

$$f_{li} = \alpha F_i + (1 - \alpha) p_{li} \quad (2.25)$$

where p_{li} is the fraction of the total sediment load transferred to the bed:

$$p_{li} = \frac{q_{bT}p_{bi} + q_{sT}p_{si}}{q_{bT} + q_{sT}} \quad (2.26)$$

where p_{bi} and p_{si} are fraction of sediment of each grain-size for bed load and the suspended load respectively.

To solve Equations 2.23 and 2.24 numerically, they are put into discrete forms. Equation 2.23 is made discrete by using a weighted up-winding coefficient (a), and looking both at the upstream and downstream bed nodes for the spatial discretization and for the temporal discretization, it uses an explicit forward Euler method. The a coefficient can be changed but a value of 0.7 is often used. This explicit method has benefits from allowing one to solve the equation directly, but forces one to employ short time steps. Solving for the bed elevation at the next time $k + 1$ for each spatial step, j gives:

$$\eta_j^{k+1} = \eta_j^k - \frac{\Delta t}{1 - \lambda_p} \left[a \frac{q_{tTj}^k - q_{tTj-1}^k}{x_j - x_{j-1}} + (1 - a) \frac{q_{tTj+1}^k - q_{tTj}^k}{x_{j+1} - x_j} \right] \quad (2.27)$$

where:

$$q_{tTj} = q_{bTj} + q_{sTj} \quad (2.28)$$

In a similar manner, Equation 2.24 is made discrete using the weighted up-winding coefficient and explicit forward Euler method.

$$F_{i,j}^{k+1} = F_{i,j}^k - \frac{\Delta t}{(1 - \lambda_p) L_a} \left[\left(a \frac{(q_{tTi,j}^k - q_{tTi,j-1}^k)}{x_j - x_{j-1}} + (1 - a) \frac{(q_{tTi,j+1}^k - q_{tTi,j}^k)}{x_{j+1} - x_j} \right) - f_{li} \left(a \frac{q_{tTj}^k - q_{tTj-1}^k}{x_j - x_{j-1}} + (1 - a) \frac{q_{tTj+1}^k - q_{tTj}^k}{x_{j+1} - x_j} \right) \right] \quad (2.29)$$

The above equation is solved for each fractional grain-size, i used to find the new fraction of each grain-size. Both equations are then solved for each loop along the reach for the next time step to

update both the bed elevation and fractional grain-size. Once this is complete, it is done for each node along the reach.

Oscillation Smoothing

Due to problems with sharp fronts forming in the bed during the update of the bed elevation, a smoothing technique was added to the program to help dissipate these sharp fronts. This follows the work of *Bhallamudi and Chaudhry (1991)*. This adds artificial viscosity to the discretization of the Exner equation as a way to dampen out these oscillations.

Calculation Check and Normalization

Once the bed elevations have been set as well as the various new grain-size distributions at each node, the program checks for errors in the numbers to determine that no null values exist anywhere. If it finds any of these values, the program is terminated. It also re-normalizes the grain-size distribution, finds the cumulative distribution at each node, as well as other important grain-size parameters like the median grain-size.

Stratigraphy Storage

This section follows the method as laid out in *Viparelli et al. (2010a)* with some modifications to account for a wider ranges of reaches used. In that paper, *Viparelli et al. (2010a)* laid out a method based on a set datum for every node in the reach. This method works well for small reaches with a low slope and flume experiments. However, once the reaches became longer with lower slopes, this method would cause an inordinate number of nodes needed especially at the upstream nodes. This large number of storage nodes needed causes the program to run much more slowly and does not provide any additional useful information to the program. I therefore specify the number of vertical storage nodes for each along-stream node by setting the distance that stratigraphy storage nodes extend from above and below the initial bed elevation. This allows for a much smaller amount of nodes needed while maintaining the stratigraphy storage.

At the start of the simulation, the program sets up the initial stratigraphy of the storage node. First, the number of nodes is set based on the integer value of twice the stratigraphy distance over the value assigned to the storage layer thickness. Then, the active layer thickness, L_a (Hirano, 1971) is calculated as:

$$L_a = n_a d_{90} \quad (2.30)$$

where n_a is the factor multiplied by the d_{90} for the active layer thickness and set as 2 in the model. The active layer is the layer that contributes to the bedload and suspended sediment load transport in each time step. This value should be less than the storage layer thickness or the storage layer thickness needs to be changed.

The model then sets the elevations at the various stratigraphy storage levels in the reach. The bottom elevation (at node 1) is set at the bed elevation minus the stratigraphy distance value. The proceeding nodes are then set as the prior value plus the storage layer thickness. This proceeds until the model gets to the flag value of the storage layer. At this point, the elevation is set at the bed elevation minus the active layer thickness. At nodes above this elevation, the elevations are set as N/A values. This allows them to be used later if there is aggradation and to serve for future storage needs. During this step it sets the partial distribution of the grain-size distribution at each node in the reach based on the input files.

After the new bed elevation has been determined, the model then updates the elevation at each node. See *Viparelli et al. (2010a)* for how this is accomplished as the model follows the formulas as laid out in that paper except for some minor modifications for both aggradation and degradation of the bed. The main difference is that instead of a bottom elevation set to the datum level as in the paper, the equations and storage elevations have been modified as laid out above in the stratigraphy set up.

This method allows the code to run much faster and have a wider variety of uses than before. The main issue with this method is that if the aggradation or degradation goes above or below the stratigraphy distance from the initial elevation, it will cause the program to fail which makes the

choice of stratigraphy distance important in the set up of the program for the expected maximum change in bed elevation.

2.2.4 Model Calibration

Results from the flume experiment were used to calibrate the hydraulics of the one-dimensional model. Experiential velocity and water surface elevations were used to help parameterize resistance terms in non-hydrostatic flow submodel so that the flow over and around the dam was better represented.

2.2.5 iRIC Interface Connection

The 1D model was incorporated to the International River Interface Cooperative (iRIC) software as an easier way for a user to access this model (<http://i-ric.org>). iRIC is a freeware hydraulic and morphodynamic set of modeling tools created by the United States Geological Survey (USGS) and the Foundation of Hokkaido River Disaster Prevention Research Center (Japan). This allows the model to function in a user friendly way with an already developed pre- and post-processing system especially for hydraulic and morphodynamic models. The user can change various model parameters to test a wide range of various scenarios then view the computation results in a visual way with a user interface (Nelson *et al.*, 2016). See Appendix A for a guide on how to run the model in the iRIC environment and for the necessary files to run the program.

2.3 One Dimensional Morphodynamic Model Runs

A series of model runs was developed in order to address the three main hypotheses. Table 2.1 summarizes these model runs. These model runs are based in part from the work of *Pearson and Pizzuto* (2015) on Red Clay Creek in Northern Delaware. This is an approximately 30-meter-wide gravel bed stream at a 0.48% slope with an old 2.5-meter-high RoR dam. The study describes in great detail the parameters of the river around the dam including the grain-size distribution. A simplified version of the reach was created as a way to better understand the controls and be able

Table 2.1: Summary of 1D model runs grouped by the main variable it was changing.

Parameter	Number of runs	High end	Low end	Unit	Notes
Sediment Supply Rate	5	10	0	kg/s	
grain-size Distribution	8	43	2	mm	Equilibrium
grain-size Distribution	8	43	2	mm	$Q_{bf} = 1.05 \text{ kg/s}$
Dam Height	8	2	0.1	m	
Discharge	8	63	10	cms	
Unsteady Flow*	14	75	5	years	
Changes with top layer	9	150	10	cms	Flow rate changes
Detailed Model	3	43	10	mm	
Flow Rate Increase	2	43	35.3	mm	
Narrow Width River	3	43	10	mm	

*The unsteady flow runs include variations in the bed median grain-size, width of the river and dam height as well as runs with a limited sediment supply for high flow events.

to parse out the various controls around a RoR dam. For the base case, the flow rate was set at 35.3 cms which is the 1.1-year return interval on flow, the mean grain-size was 28.8 mm which makes this a gravel bed river. The dam height was set at 1.6 m tall with sloped walls similar to that described in the flume experiment. The dam sat at 1000 m along the reach with a total reach length in the model of 2000 m. For the most part, nodes (or cross sections) were set at every 10 m except at areas around the dam where they more closely spaced to better capture the hydraulics and bed elevation change. The below parameters and values were systematically varied to address the hypotheses presented above. The goal was not to specifically model the RoR dam on Red Clay Creek, but to use this well-documented example of a RoR dam as a realistic test case to determine the various controls on these dams.

The first group of runs explored how sediment supply variations affect the amount of sediment stored above a RoR dam. To accomplish this, sediment supply rates were varied while the other parameters were kept constant. The grain-size distribution and supply rate for the run was determined by taking the equilibrium grain-size distribution and supply rate and using this as the base case with a sediment bed $D_{50} = 28.8 \text{ mm}$ and a supply rate of 4.94 kg/s . Additional runs doubled the supply rate (10 kg/s), halved the rate (2.5 kg/s), used a lower value (1.0 kg/s), used the annual rate as given in *Pearson and Pizzuto (2015)* (0.47 kg/s), or used no sediment supply rate (0 kg/s).

The next set of runs dealt with the variations in grain-size distribution of the supply rate. The base case for this model was based on the equilibrium sediment rate. The variations were based first on making the D_{84} and D_{16} of the original GSD the new D_{50} while keeping a similar shape to the GSD so that the new D_{50} is 43 mm and 10 mm, respectively. In addition, the following D_{50} of the GSD were added as a way to increase the variety of cases. The median grain-size varied from 2 mm (at the gravel-sand transition) to 43 mm. In addition to runs with a wide variation of sizes in the base material, a run was created with a single grain-size of 28.8 mm to see the effects of a single grain-size. See Figure 2.2 for the different grain-size distributions that were being used.

The sediment supply for the latter set of runs was calculated as the transport capacity, depending on the flow rate and the upstream bed grain-size distribution. This created variations in the upstream sediment supply rates. To control for this variable, a group of runs with an armored subsurface (stratigraphy layers below the active layers) and a constant sediment supply rate were used. The GSD of the supply rate was computed based on the GSD of the run in the later group of runs. The supply rate was set so that there would be no upstream aggradation in any of the runs. This group was run for each of the median grain-sizes as stated above and as shown in Figure 2.2.

Another group of runs varied the (constant) flow rate. The upper end was based on the 2 year flow at 63.7 cms. The lower end was set at 10 cms where bedload was just barely being transported. The remaining values were in between so that all the flow rate values were 10 cms, 15 cms, 20 cms, 25 cms, 30 cms, 35.3 cms, 48 cms, and 63.7 cms.

The final set of runs used to address the first hypothesis varied the dam height. In the base case, the dam was set at 1.6 m. The dam height was thus varied from 0.1 m to 2.0 m with a bigger focus on looking at the variations in the dam height at the lower heights.

The second hypothesis ask whether high flows are able to scour out the sediment behind the dam. A nearby USGS gage has about 75 years of daily flow data (USGS, 2018) which were used to generate the return period flows as told above and described in *Pearson and Pizzuto (2015)*. These data were used to investigate the impacts of unsteady flow of channel morphology and reservoir scour. In some cases, the model was run for five years of daily data. For other cases, the data was

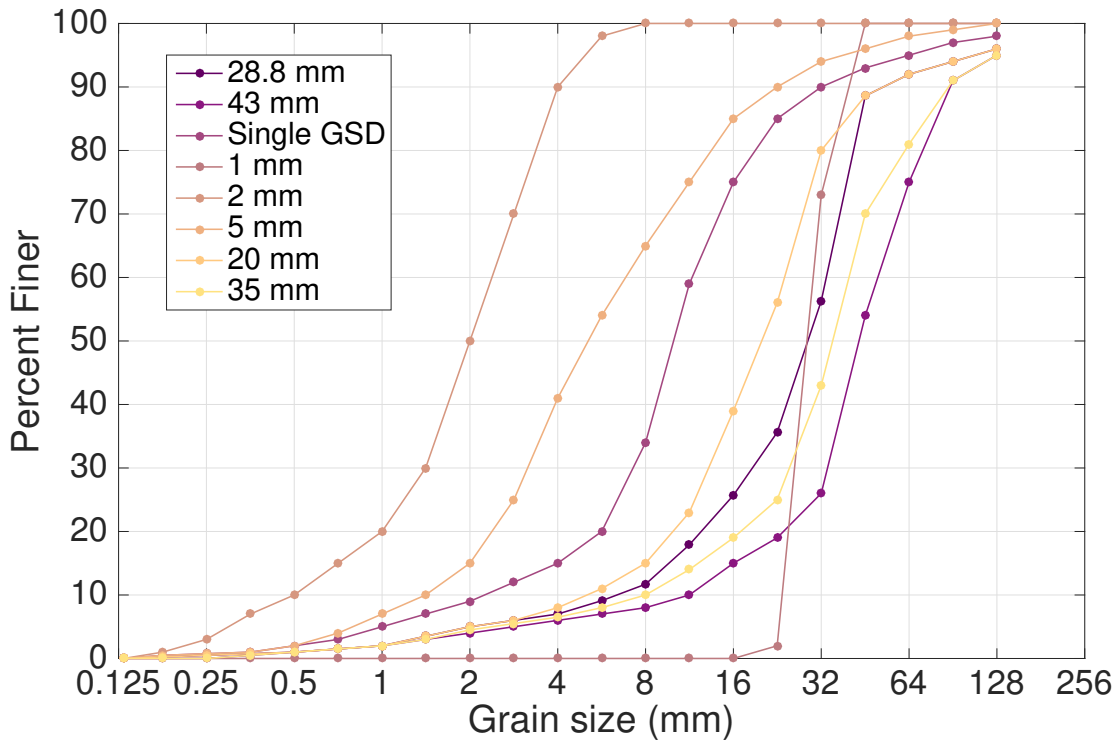


Figure 2.2: Cumulative distribution function of grain-size distribution of the bed material for different runs. The 28.8 mm GSD is used as the base bed material for the majority of the model runs.

run for the entire time period of approximately 75 years. In addition, some of the unsteady runs changed the base grain-size distribution, the model width or the dam height. In addition, a series of runs were conducted in which the flow rate increase by 1 cms every day to see how the system responds to gradually increasing flow.

Another group of runs investigated the third hypothesis, which concerns the storage efficacy above the dam. In addition to the runs described above in which the dam height varied, a set of control runs with no dam were used to isolate the effect of the dam relative to a scenario where there is no dam impeding the flow.

I also created a more detailed model of the Red Clay Creek based on *Pearson and Pizzuto* (2015) for comparison against the simplified models described above to see if the simplified nature of these runs affected the general findings of the study. I conducted a set of runs using different

channel widths to see the effects that a narrower width has on the storage efficacy and have a model that can move bedload at all times in the model run.

Overall, these runs took a little over two hours to run for approximately a year run time at a 30 second time step using an Intel Xeon CPU E5-2687W v3 @ 3.10 GHz processor on a single thread (out of 20 total). This allowed many different runs to be concurrently run on the machine. Some of the longer unsteady model runs (75 years) took around two weeks to run. Several runs were done at a five second interval which also increased the run time. The run time does not increase linearly due to increased memory and processing power in the models with the longer run times. In total, approximately 70 of the dam models were completed with a similar run time for the no dam control model runs.

2.4 Two Dimensional Morphodynamic Model Runs

In order to see if there are significant differences when moving from a 1D to a 2D model, a few simulations were conducted with NAYS2DH (*Nelson et al.*, 2016). This model runs in the iRIC interface as described above and allows for unsteady and steady gradually varied flow computation with the 2D shallow water equations. It can compute both bedload and suspended sediment transport with varying mixed grain-size equations. Due to the long run times of a 2D model, only three models were run in a similar set up to the base model run described in the 1D modeling section.

Chapter 3

Results

3.1 Flume Experiment Results

3.1.1 Water Surface Measurements

For a view of the experimental setup with the flume and the dam as well as the curvilinear flow present for the flow see Figure 3.1. This view shows an example of the model run and gives a sense of how the water flows over the dam.

Figure 3.2 shows the water surface profile around the dam with the slope and a view of the dam for the test runs of different discharges with the flow based on the orifice plate reading. The blue lines in each case are for the no backwater case. This shows how the curve of the flow over the dam increases as the discharge increases in both height and total curvature. In each case, the dam causes backwater to form on the upstream side where the flow could be considered gradually varied flow. The steep slope (1.18%) of the reach makes the flow profile on the upstream side a S1 flow profile (*Chow, 1959*). As the flow approaches the dam, it becomes more rapidly varied in nature and approaches critical depth in each case. As the flow goes over the dam for the case of no downstream backwater, it becomes supercritical with a curved water surface profile. It stays supercritical for each flow discharge as it exits the flume back into the water storage tank. For Run A, measurements were not taken frequently enough which makes the water surface line appear to go through the base through the dam.

As the backwater effects on the downstream side were increased through the use of the sluice gate control, the return to supercritical flow downstream of the dam no longer happened. At first, the curve would remain and the flow would drop down to a subcritical flow section. As the flow increases more, the effect of the dam becomes washed out to the point of where the water surface does not change much as it passes over the dam. The various backwater profiles and how they change are shown in Figure 3.2. Run 2 is not shown in these as water surface measurements were



Figure 3.1: View of the experimental set up in the flume with the dam and the curvilinear flow over the dam in the case of where the discharge is 0.16 cfs (Run B.1).

often not repeated as nothing changed around the dam. Run D.2 is more similar to the Run 3 for the others and Run D.3 is more similar to Run 4 for the other flows. In addition, Run C.3 lack of change is based on the hydraulic jump moving downstream after measurements were performed upstream. The large changes caused by small changes to the downstream sluice gate on the degree of submergence made it difficult to have much more consistency among the runs.

3.1.2 Velocity Measurements

Approximately 300 measurements of velocity were conducted for the different discharges and backwater effects around the dam. The results show expected trends in the downstream velocity profile such as the Law of the Wall in most cases. For each flow profile taken, the average velocity was found and this was used to estimate the discharge as a way to validate the orifice plate. Overall, the results tend to match up well. This shows that generally the orifice plate provides accurate enough results of the discharge so that it can be used without the need of having to back calculate the discharge or measure the discharge in another manner.

For the final experiment, run D.3, much more detailed velocity profiles were taken behind the dam, over the dam and just downstream of the dam compared to that of any other experiment. See Figure 3.3 for the three velocity distributions. These include both the downstream (x) velocity and the vertical velocity (z) to preserve the magnitude and direction of each velocity. The velocities are

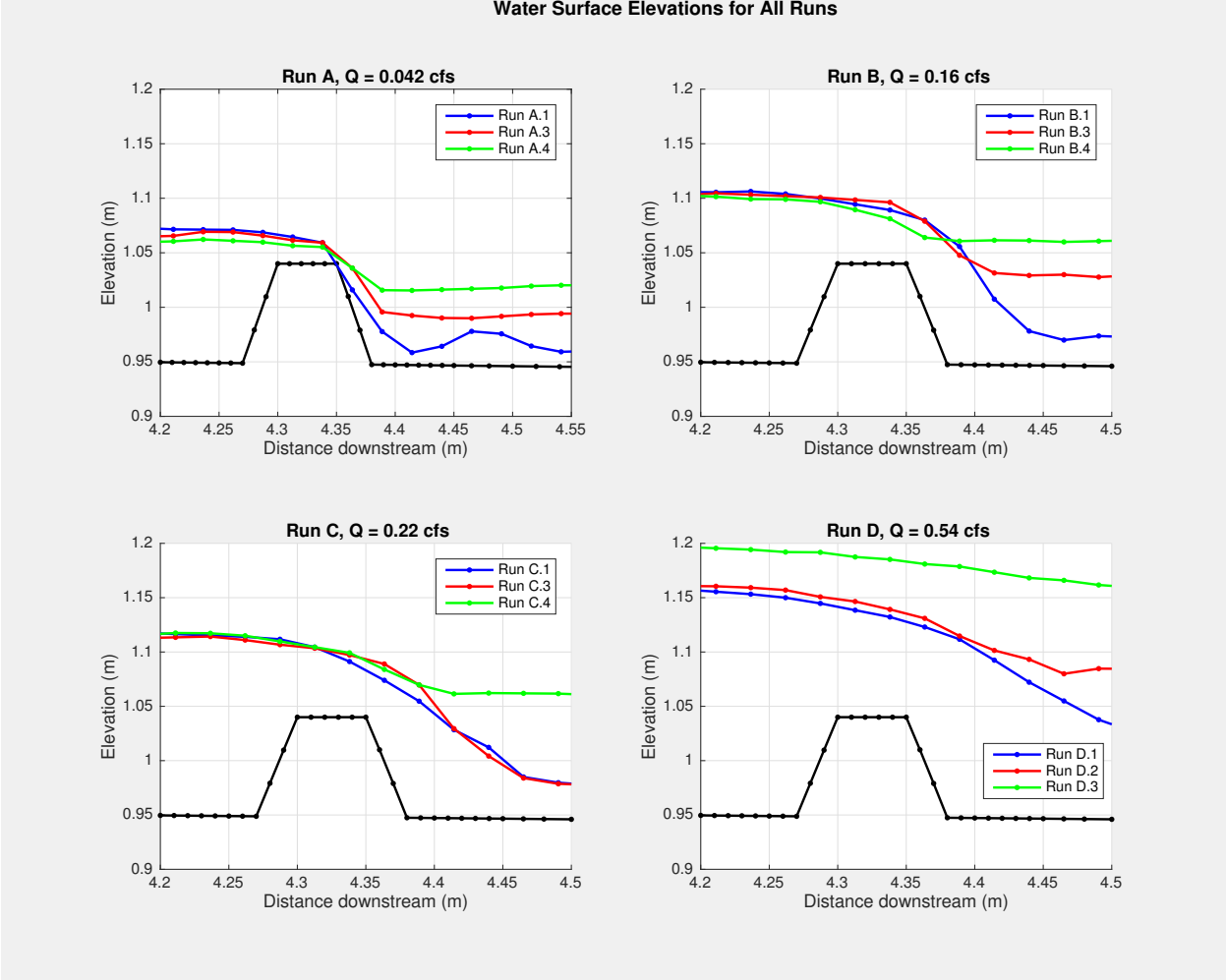


Figure 3.2: Water surface elevations of the four experiments and each backwater condition that changed the local dam water surface elevation.

scaled as noted in the legend and the water surface elevation is shown as well. The circular motion downstream of the dam can be seen as the near-bed velocity is oriented upstream, with a slightly upward trajectory.

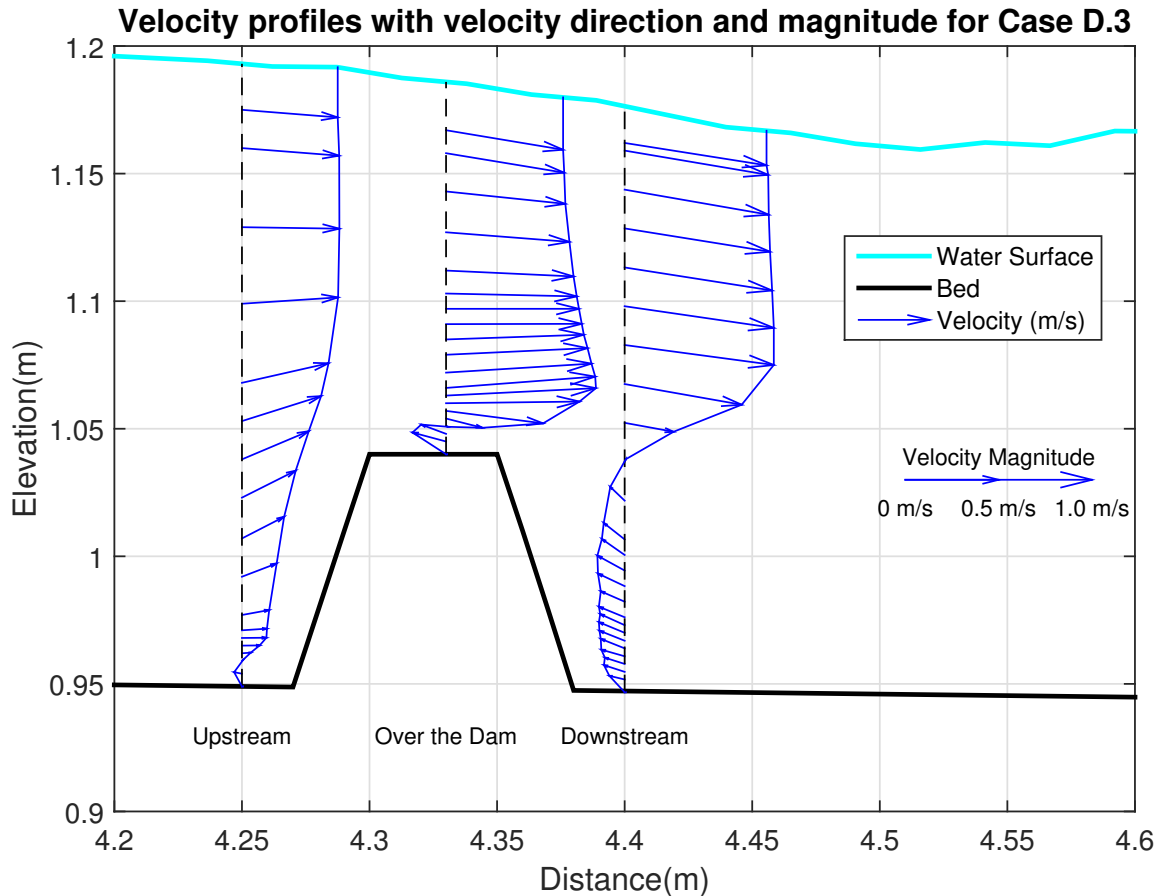


Figure 3.3: Detailed velocity distributions around the dam for Run D.3 showing the vertical and downstream velocities as well as the resulting direction and magnitude in the vertical profile with the water surface elevation included.

3.2 One Dimensional Morphodynamic Results

3.2.1 Flume Calibration Results

Figure 3.4 shows the measured water surface elevations for the flume experiment with no back-water compared against model-predictions of the water surface. The model clearly calculates a non-hydrostatic curvature of the water surface over the dam. For low flows, the model predictions

and experimental observations match up well, but for higher flows the model tends to over predict the depth, especially downstream of the dam.

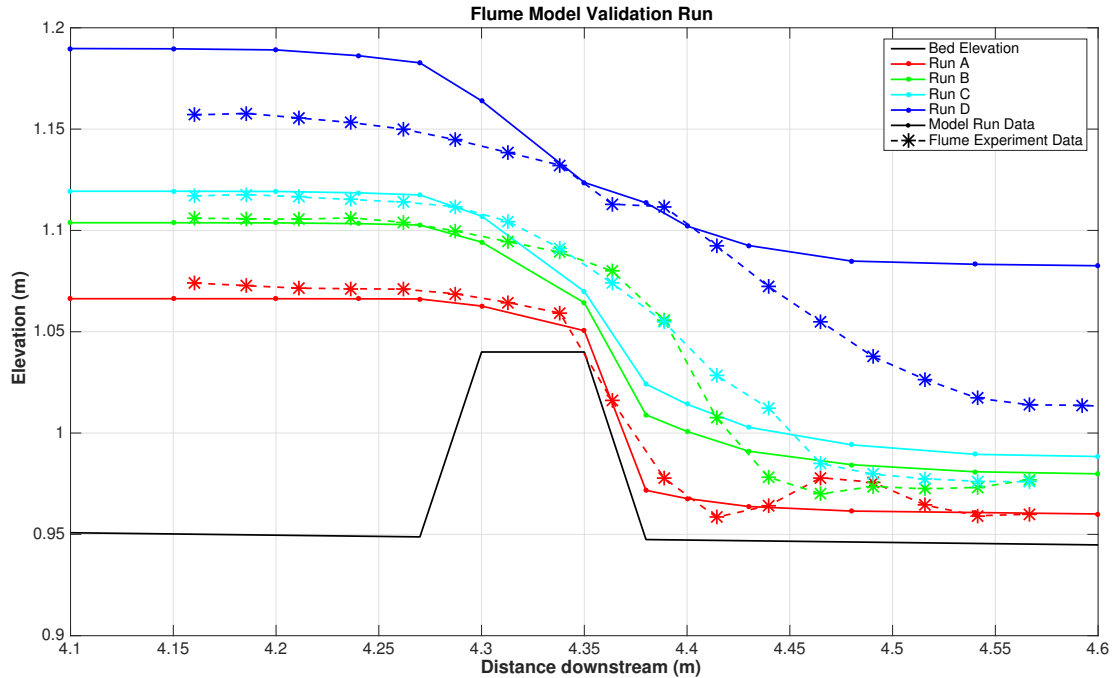


Figure 3.4: Validation of one dimensional model with the results of flume experiment with the flume experiment results in dashed lines and the model results in solid lines.

3.2.2 Model Runs

Figure 3.5 shows the results of the base model with the dam at 45 days. This shows the water surface elevation at the current time and the elevation of the bed as well as the stratigraphy of the mean grain-size. Note the aggradation upstream of the dam and the sequence of stratigraphy with the varying grain-sizes. On the downstream end, note the degradation and how the mean grain-size increases just downstream of the dam.

Changes in upstream sediment supply

Figure 3.6 shows how changing the sediment supply rate affects sediment storage upstream of the dam. As shown in the figure, after 300 days in some cases the model reaches equilibrium in

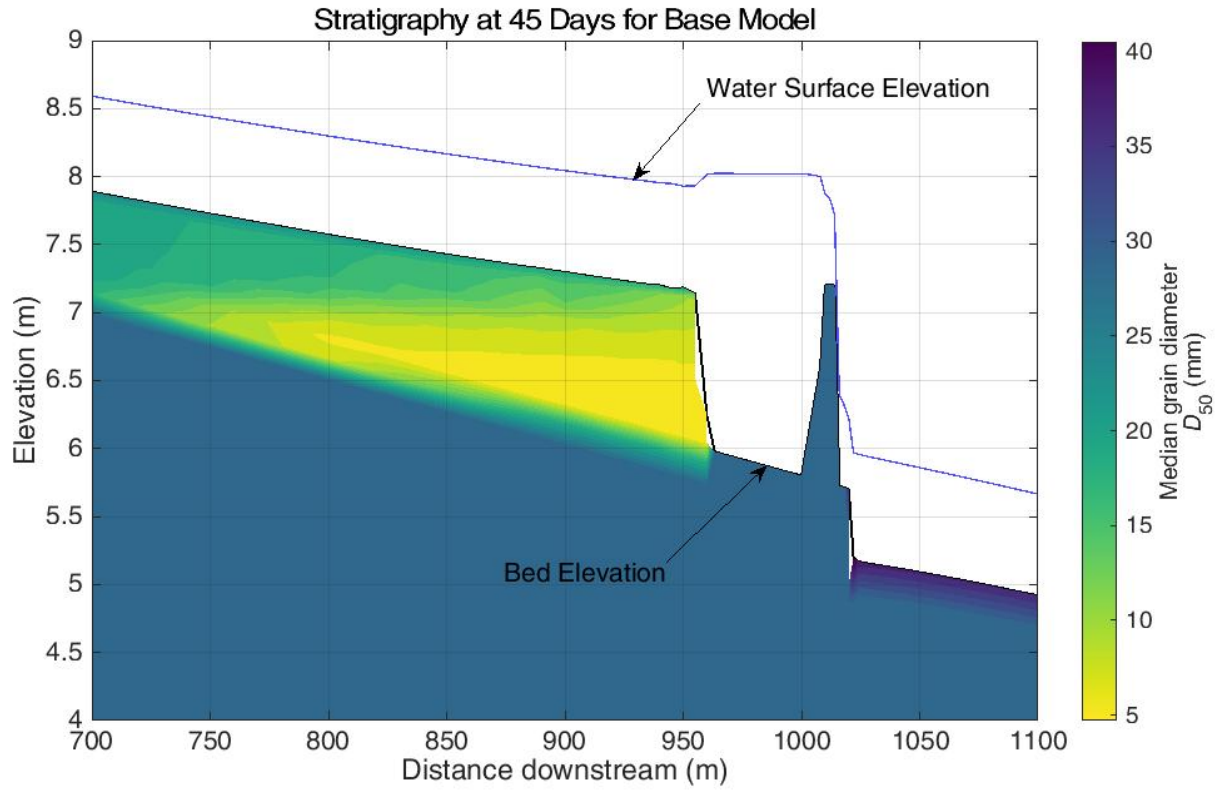


Figure 3.5: The base model run at 45 days with the water surface elevation and median grain diameter for the various stratigraphy layers around the dam. Note the differences in the x and y scales.

which the sediment being stored above the dam is equal to the rate at which it is exiting the dam. The sediment storage increases approximately linearly with time during the the initial filling, until it reaches a point where it dramatically slows. At this point, some sediment is passed over the dam. After a long time at any of these rates, equilibrium eventually reached. As the upstream sediment supply rate increases, the rate of sediment being stored upstream of the dam also increases. In addition, the upstream stored sediment affects the total amount of sediment that is stored above the dam. Figure 3.7 shows how bed elevation evolves over time at three different locations. The first

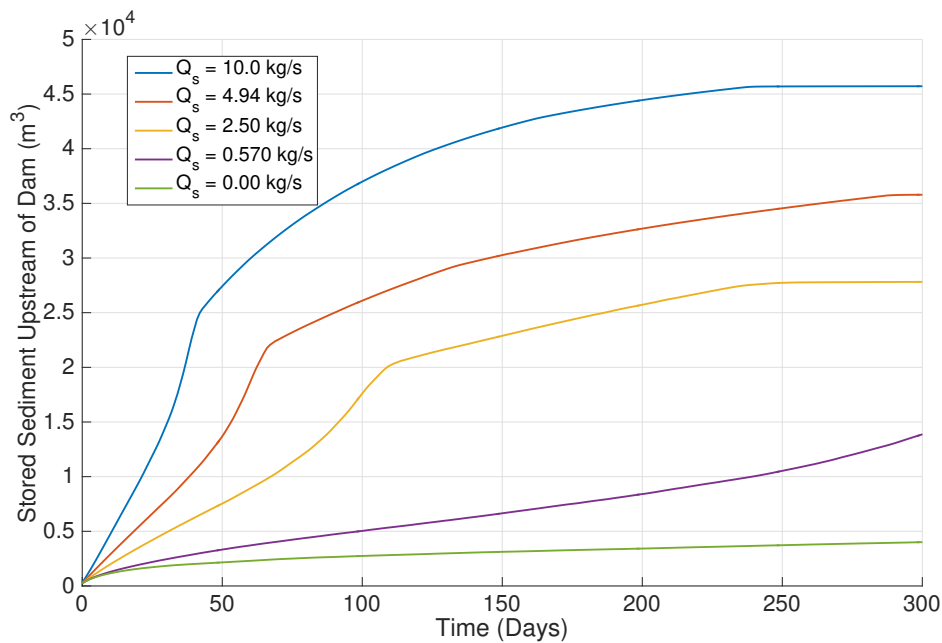


Figure 3.6: Amount of stored sediment over time for the set of runs with changes in the upstream sediment supply rate.

location at 710 m was chosen as the initial bed elevation here is approximately equal to that of the top of the dam elevation for flow rate of 35.3 cms. The midpoint location was taken as the midpoint between the other two locations in terms of total nodes at 925 m. The dam location was taken at the node just upstream of the start of the dam at 998 m. On the upstream end, the initial response is fast changing that slows down as it aggrades. The lines with a higher sediment supply increase at a greater rate and go to a higher change. At the midpoint, and downstream side, the response (as the foreset fills the dam) is delayed. These two have a more immediate response in terms of

the total change as the sediment aggrades. In terms of the mean grain diameter, it initially remains at the initial value as no bedload can be transported. Once the bed starts to aggrade, the initial distribution has a lower median that goes to a higher median value again that generally appears to be finer than the initial value.

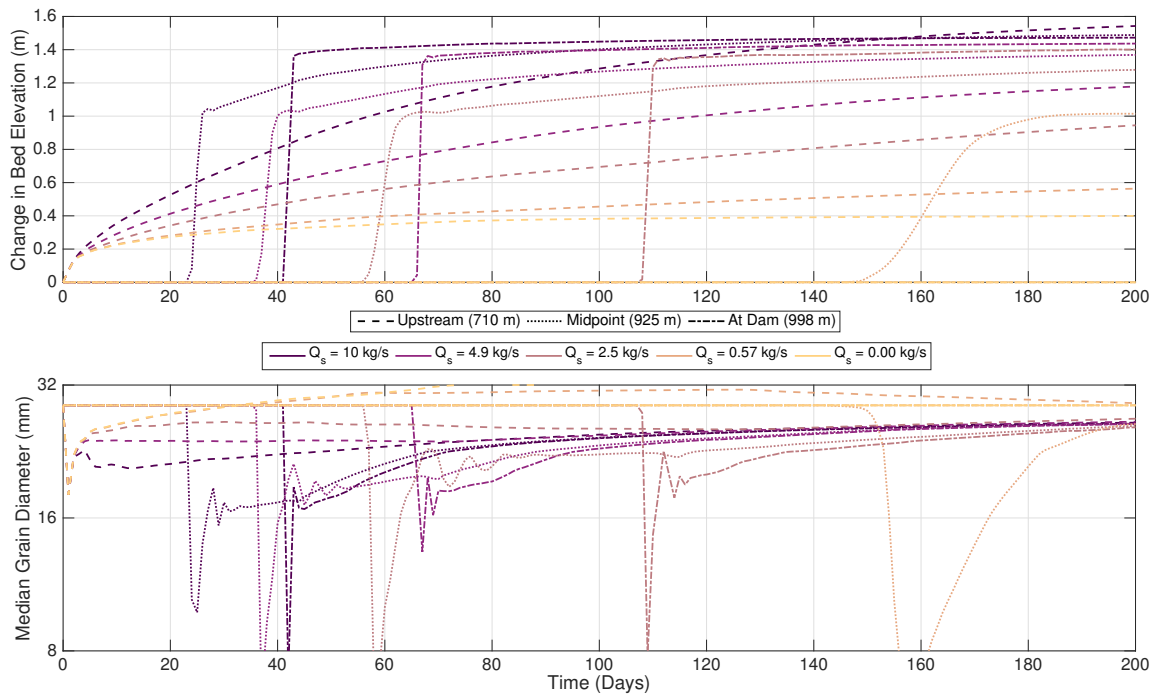


Figure 3.7: The changes in the bed elevation and the median sediment grain-size upstream of the dam in three locations over time for the case of changes in the upstream sediment supply.

Shifting the focus to the downstream effects, the more general trends are evident (Figure 3.8). This shows the downstream effects (just downstream of the dam) for both changes in upstream sediment supply and dam height for the changes in bed elevation and the median grain-size over time. The area experiences degradation until bedload is passed over the dam where the bed elevation increases to a relatively unchanging value. All of the paths on this chart follow the same initial line until bedload starts and sediment is passed over the dam which is why these were grouped together. Looking at changes in the median grain diameter, at first the bed quickly armors and

increases in size. After bedload starts to pass, the mean grain-size increases just downstream of the dam.

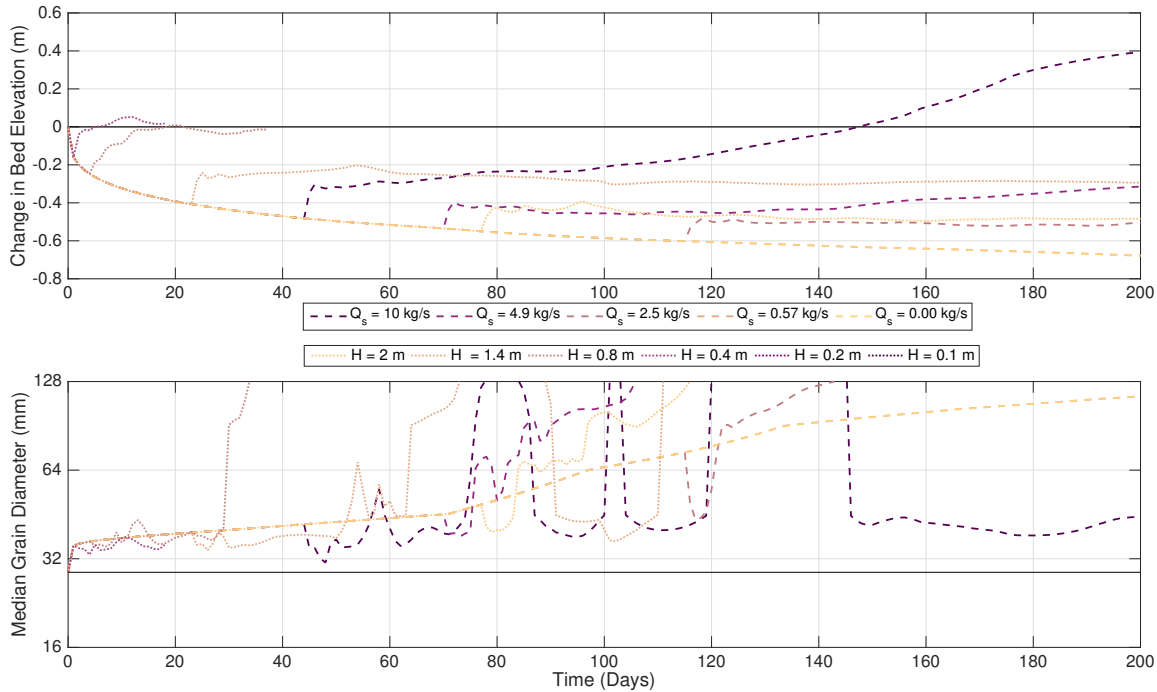


Figure 3.8: The changes in the bed elevation and the median sediment grain-size just downstream of the dam over time for the case of changes in dam height and changes in the upstream sediment supply that are grouped for similarity of the response. The dashed lines show changes in grain-size (Q_s) and the dotted lines show changes in dam height (H). The black solid lines show the initial conditions of no change in bed elevation and a median grain diameter of 28.8 mm for the top and bottom charts respectively.

Changes in grain-size distribution

See Figure 3.9 for the results of how changes in the grain-size distribution and median grain-size effect how sediment is stored over time for the model runs where the sediment supply rate varied as a way to maintain equilibrium conditions. Similarly, Figure 3.10 shows the results of changes in grain-size distribution and median grain-size effect how sediment is stored above the dam for the cases where the sediment supply rate is kept constant for the experiment duration to better see the impacts of changes in grain-size distribution alone.

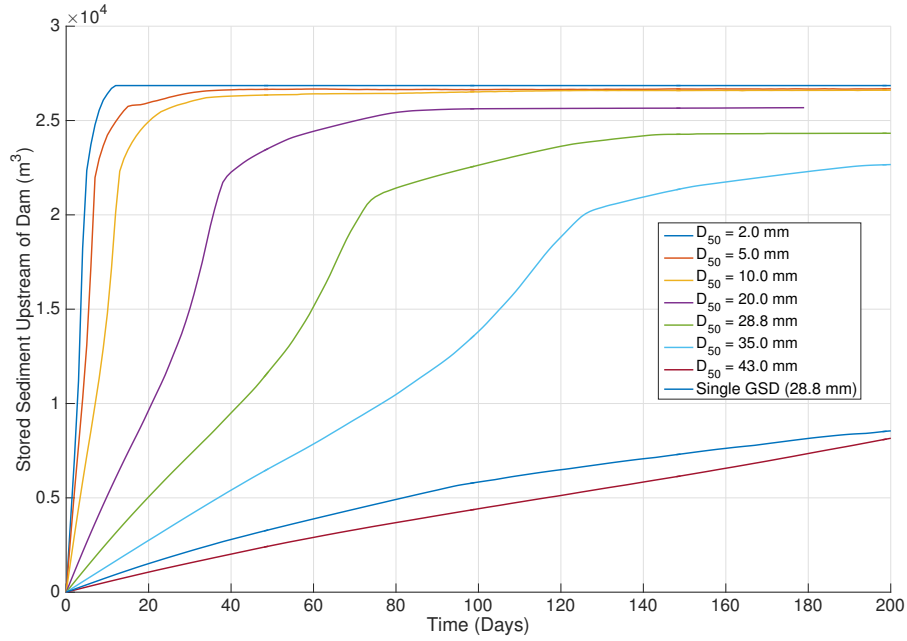


Figure 3.9: Amount of stored sediment over time for the set of runs with changes in the bed grain-size distribution and median grain-size for the case of maintaining equilibrium conditions upstream.

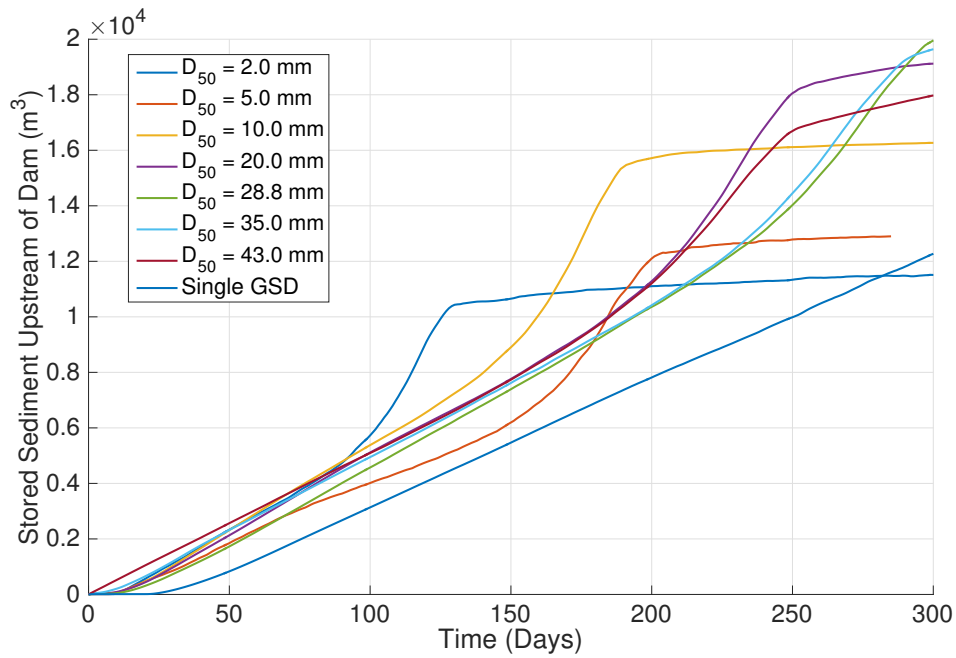


Figure 3.10: Amount of stored sediment over time for the set of runs with changes in the bed grain-size distribution and median grain-size for the case of maintaining constant upstream sediment supply rates.

Changes in dam height

For how sediment storage behind the dam changes for variation in the dam height, see Figure 3.11. Similar to the other figures, this shows how the sediment builds up over time for the dams. The biggest difference lies in how the different dam heights fill due to the vastly different amount of storage for sediment that can exist behind the various dams.

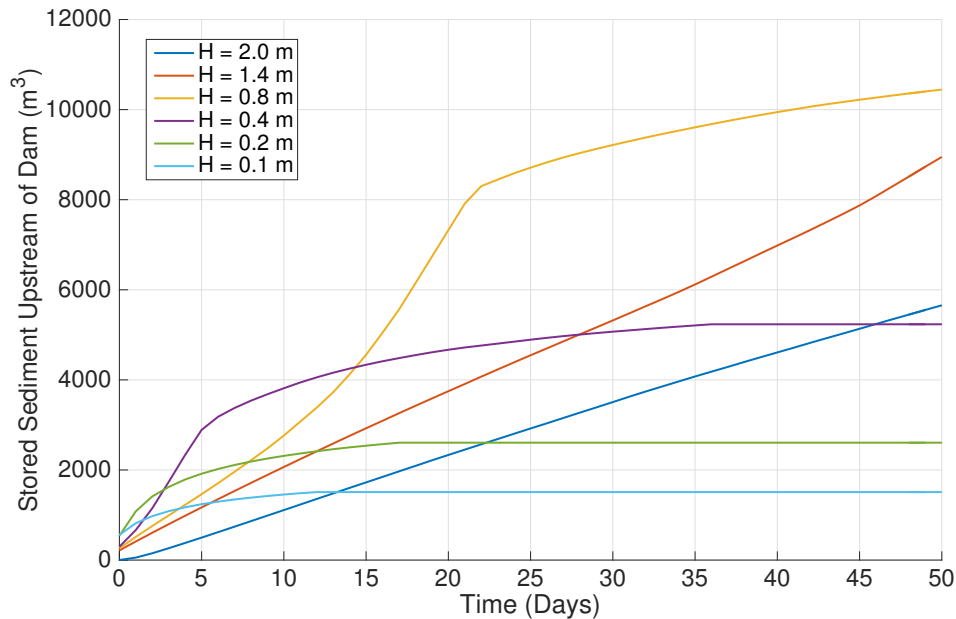


Figure 3.11: Amount of stored sediment over time for the set of runs with changes in the height of the dam.

Changes in steady discharge

See Figure 3.12 for a view of how sediment is stored behind the dam in the case of changing constant discharge. The overall trend of these lines follows the previous trends as already noted.

For an overview of all the various control parameters (grain-size distribution, dam height, upstream sediment supply and flow rate), see Figure 3.13. This shows the maximum sediment storage above the dam for each parameter to help better understand the controls on the quantity of sediment that gets stored upstream of the dams. For the upstream sediment supply, it approaches a maximum volume of storage upstream. For the dam height, the trend appears linear between stored sediment and dam height.

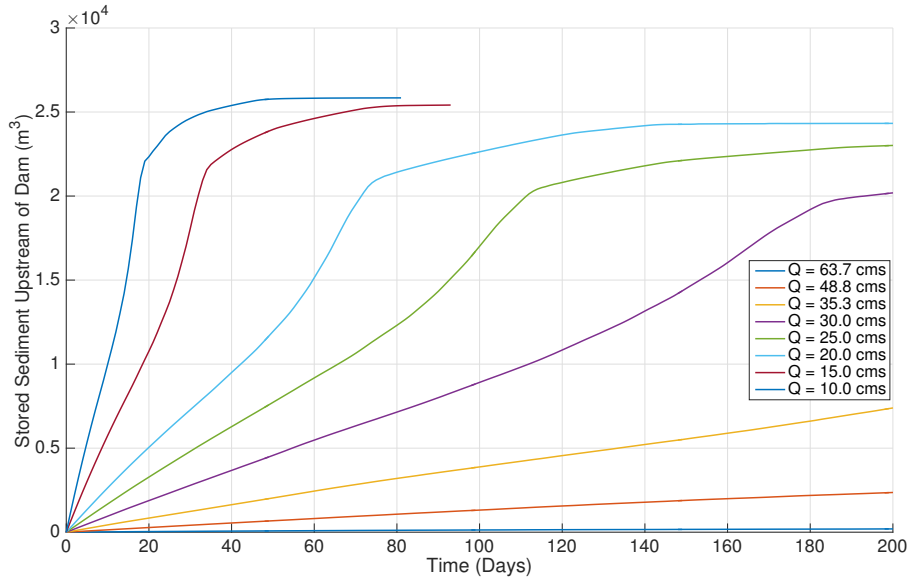


Figure 3.12: Amount of stored sediment over time for the set of runs with changes in the steady discharge.

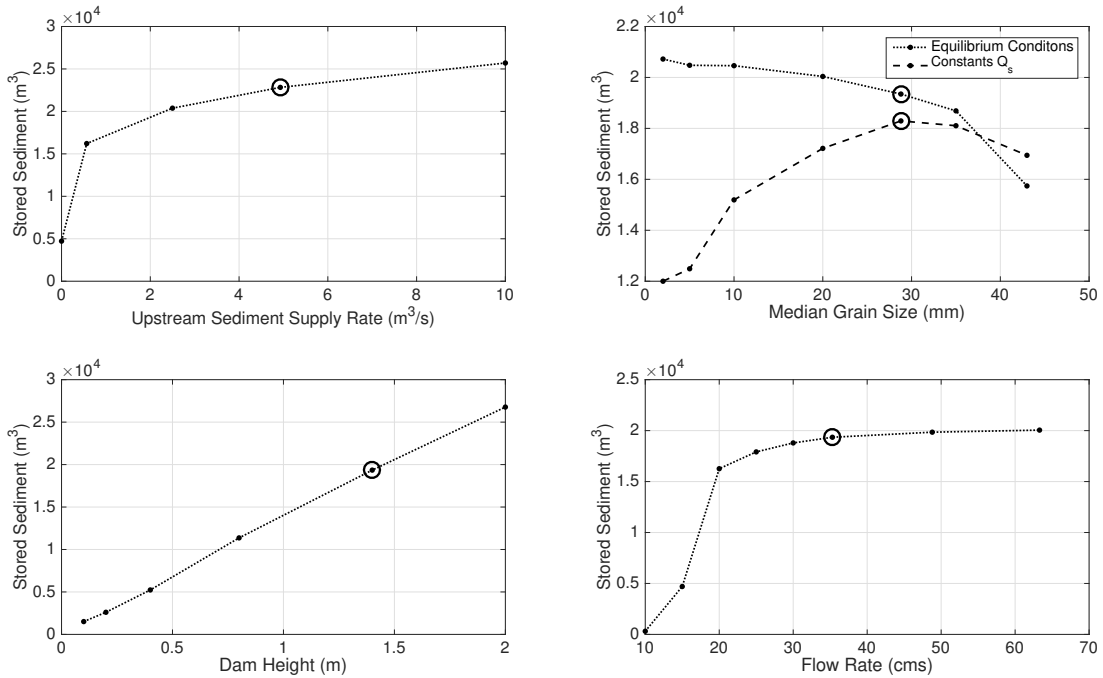


Figure 3.13: The maximum amount of sediment stored above the RoR dam for the control parameters of upstream sediment supply rate, median grain-size, dam height, and flow rate. The open circle provides the base condition for the set of runs.

More detailed model runs

The runs modeled after a more accurate and detailed model from *Pearson and Pizzuto (2015)* produced results that did not differ that much from the more simplified models. The dam filled up in a similar manner but did take a longer time period. On the downstream side, armoring and a bit of degradation occurred. As a note, the downstream bar placed in this model quickly washed out in all of the model runs to create a more uniform downstream slope.

Unsteady flow runs

These runs gave a wider variety of results depending on the various parameters changed such as dam height changes, reach widths, and median grain-size changes. Figure 3.14 shows the summary of how the reservoir in each unsteady run gets filled over time. These models tend to show increases in the total amount of stored sediment as it fills up the dams. Eventually as the dam fills up, the total storage goes to an equilibrium conditions where the total sediment stored does not change much. In some cases, there appears to be a bit of scouring meaning that the reach loses sediment stored upstream of it. In these cases, the amount of loss is minor in terms of the overall sediment above the dam. This only includes runs with higher amount of sediment storage and in order to better see all the relevant unsteady model runs, refer to Figure 3.15. This shows the stored sediment over the maximum amount of stored sediment over time for each run to better compare how each run fills the area behind the dam relative to the maximum amount of storage for that run. The majority of these do not experience times with removal of sediment behind it except in the clear case of a mean grain-size of 43 mm for the surface, on a narrow river with a limiting sediment supply for high flows. This run showed the clear trend of reducing sediment during periods of high flow events. Due to this trend, the next figures explore in more depth this run to better understand the dynamics of scouring of sediment during high flow events.

In one of the model runs with both a narrow width reach (5 m) and a restricted sediment supply rate for higher flows, sediment fills in the dam area and then scours out during some higher flows. See Figure 3.16 for a chart from 40 - 50 years of both the flow data and the volume of sediment behind the dam. The 10-year period illustrated in the figure shows how the sediment gets filled

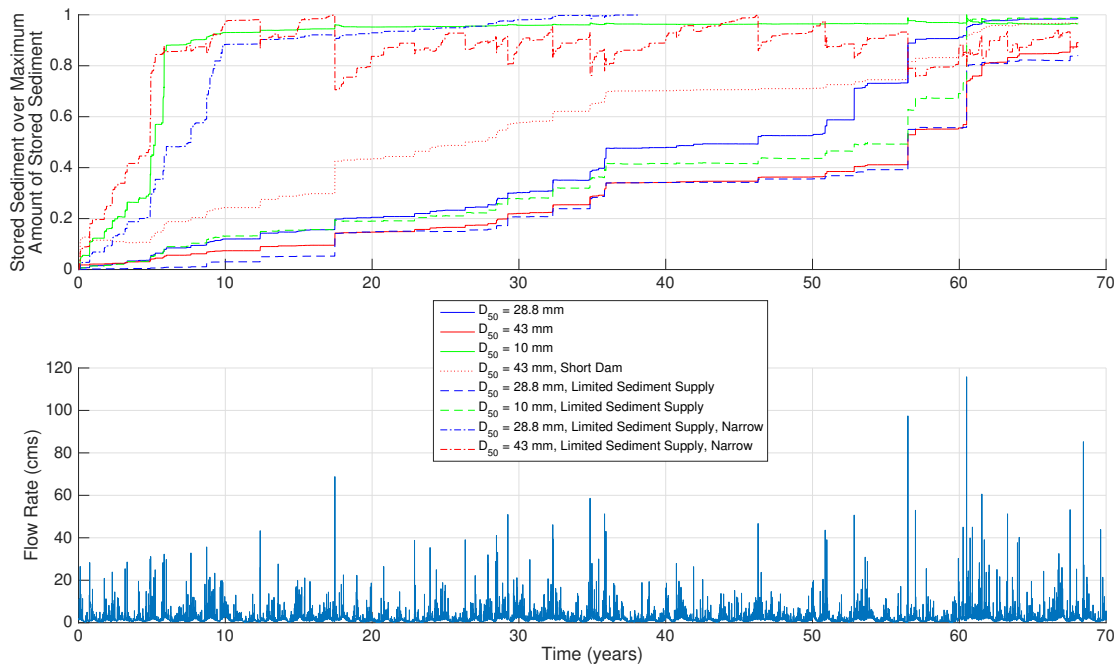


Figure 3.14: Stored Sediment over time above the dam from the time of 0 - 70 years in the simulation for the selected unsteady flow runs based on changes in grain-size, dam height, limiting of the sediment supply and the width of the river.

and scoured out with changing flows. Figure 3.17 shows how changes in the fill rate (change of sediment volume over time) relate to the flow rate where the points are colored by the total volume of sediment in the dam just before the flow rate change. This figure only shows points where the sediment changed by greater than $2 \text{ m}^3/\text{day}$ as a way to better see the locations of larger change. For lower flows (below 21 cms) only aggradation of sediment behind the dam occurs regardless of the amount of stored sediment behind the dam. During periods of moderately high flows (between 21-35.3 cms), aggradation is present when the amount of stored sediment is low while scouring takes place when the amount of stored sediment is higher. At higher flows (above 35.3 cms), all the flows scour out sediment upstream of the dam.

Narrow width model runs

The set of narrowed width models showed that sediment could be passed for the RoR dam at all periods (given a high enough flow) and did not require the longer filling time to reach equilibrium.

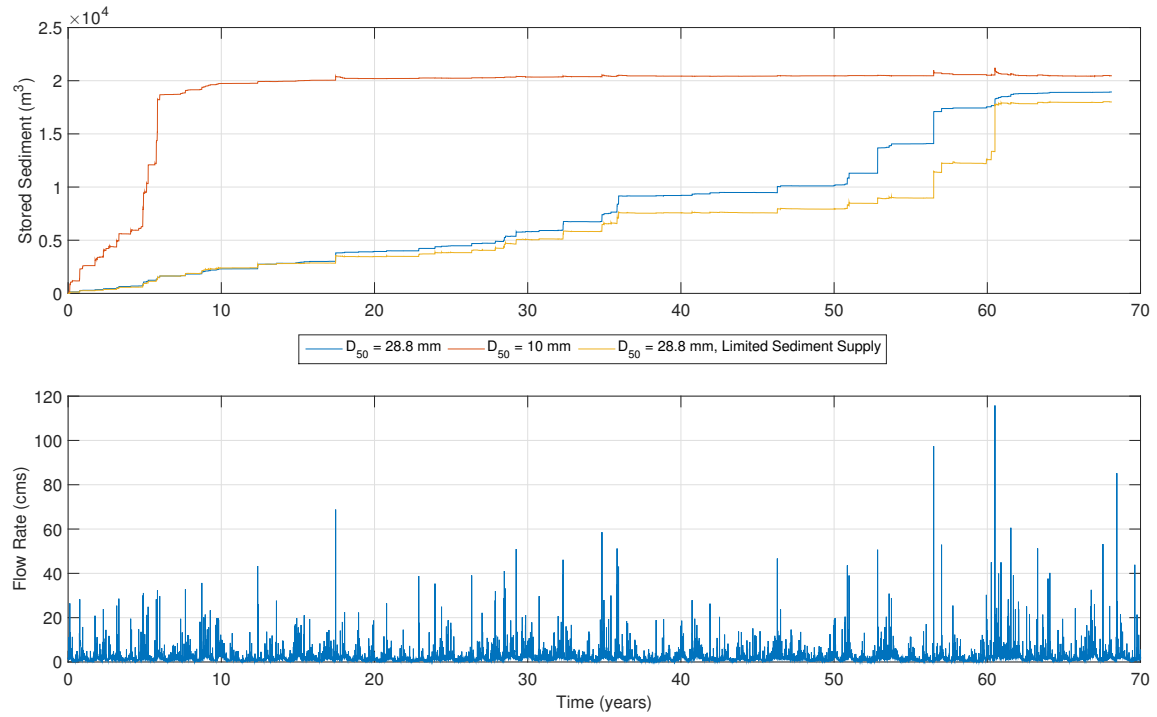


Figure 3.15: Stored Sediment over time above the dam and the flow rate from the time of 0 - 70 years in the simulation in the case of the normal reach with two different mean grain-sizes for comparison and sediment limited model run.

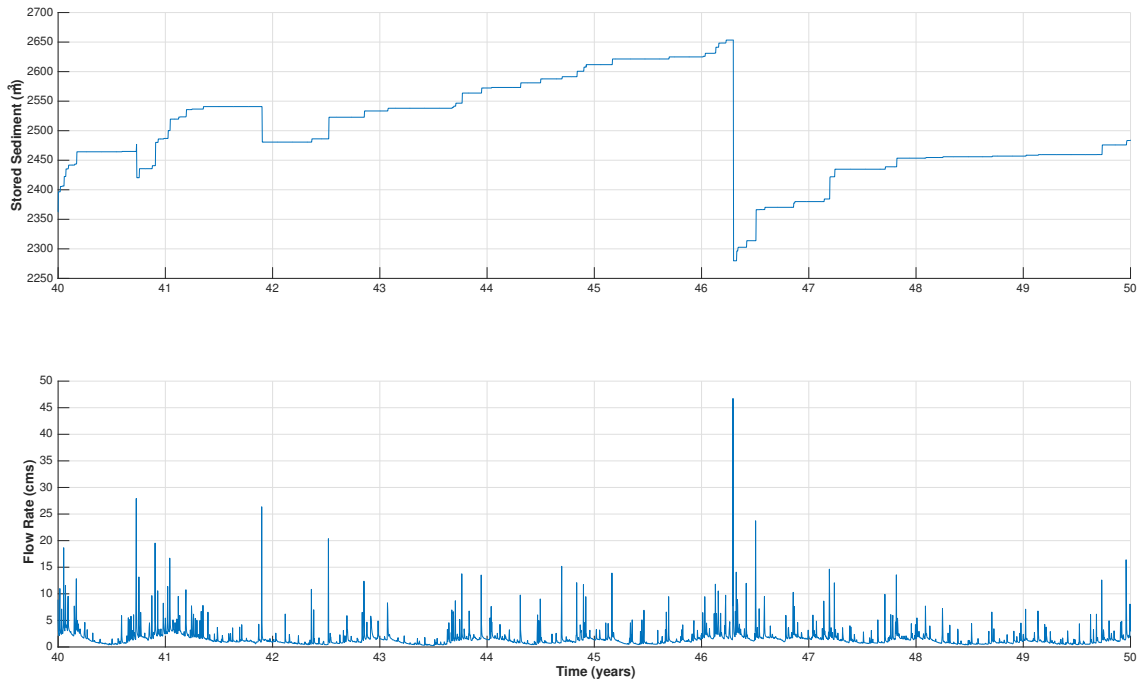


Figure 3.16: Stored sediment over time above the dam and the flow rate from the time of 40 - 50 years in the simulation in the case of a narrow 5 m reach width and limitations in sediment supply at high flows.

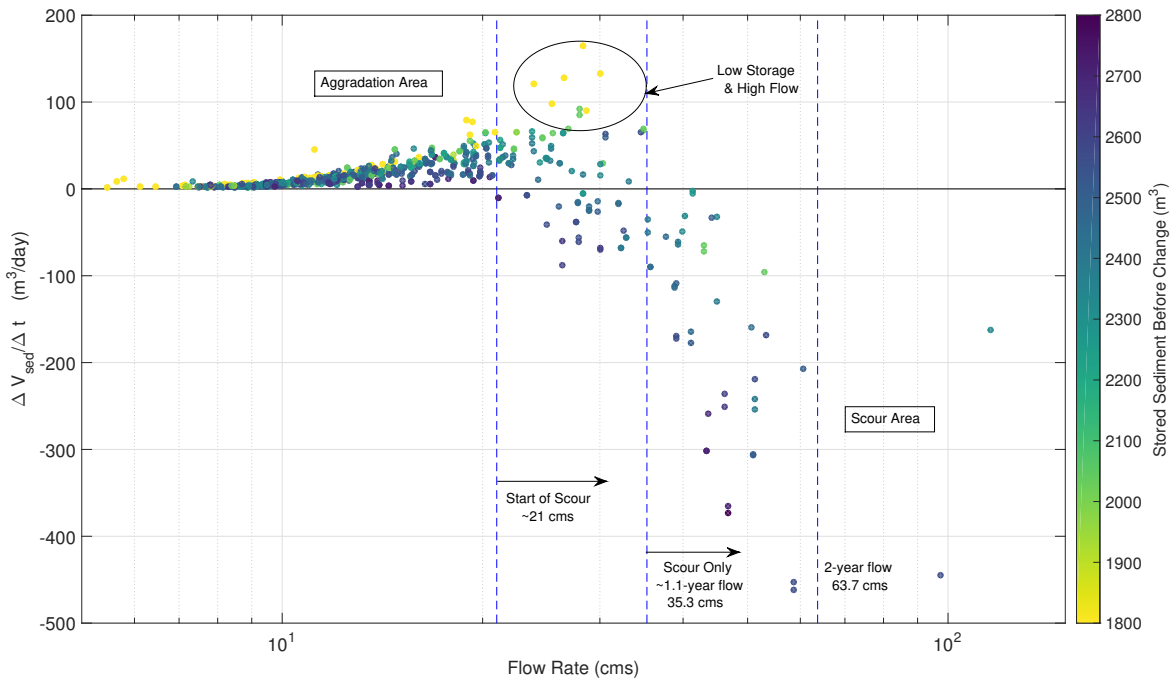


Figure 3.17: The change in stored sediment over time upstream of the dam versus the flow rate colored by the total volume of stored sediment upstream the dam right before the change to this new flow rate.

Some of these runs were done with unsteady flow such as described above. A particularly interesting run was performed where the flow was increased by one cms each day as shown in 3.18. For this simulation, after the reservoir fills with sediment higher flows start to scour out the sediment from the lower flows. As the flows continue to increase, more and more sediment becomes evacuated from behind the dam. On the downstream side, before the bedload passes over the dam, a lot of degradation occurs immediately downstream of the dam. As the sediment starts to pass over the dam, this degradation fills in a bit, yet the higher grain-sizes still remain but decrease and move downstream as the flow increases.

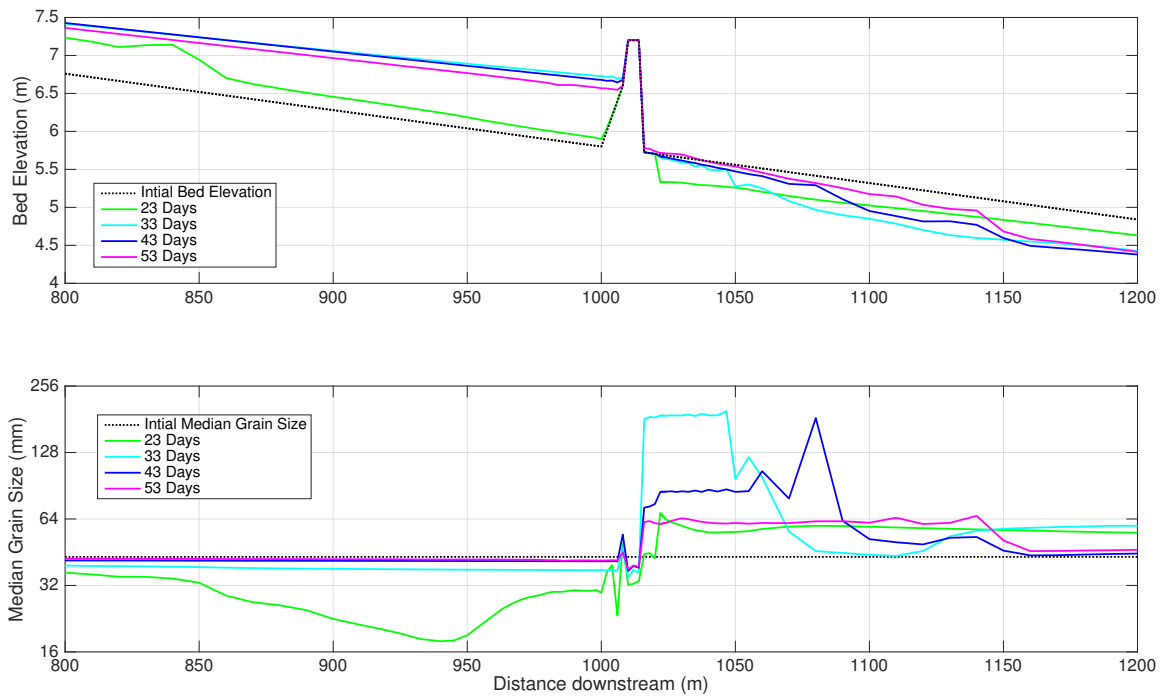


Figure 3.18: The changes in bed elevation and surface median grain-size over time for increases in flow by one cms a day at the initial elevation, 23 cms, 33 cms, 43 cms, and 53 cms.

3.2.3 Comparison to models with no dam

The majority of the models had a companion model that involved all the same conditions with the exception of removing the dam as to see the impacts that the dam had on the reach in

comparison to a reach without any dam. The models using equilibrium sediment supply did not experience any (or mild) downstream changes. Thus, any downstream variations in the models with the dam come from the dam are solely due to the presence of the dam.

The models with varying sediment supply did show changes especially on the upstream end. These show that runs with low sediment supply experienced upstream degradation and a high sediment supply showed some upstream aggradation. In addition, looking at the bed surface shows that the top layer has a higher median grain-size than just below which shows some armoring in these models.

In the differences between models with a dam and those without, we could see the changes that resulted from the dam over time. In addition, the lack of changes helps to understand the upstream and downstream effects better. As many of the models did not change, it helped to confirm the changes on the downstream side such as degradation and armoring better. The upstream side showed changes with the addition of the sediment wedge and varying grain-size distribution underneath it.

3.3 Two Dimensional Morphodynamic Results

The results from the two dimensional model show the pattern of upstream aggradation starting at the upstream end of the backwater zone effect. See Figure 3.19 for the changes in bed elevation and mean grain diameter over time. The initial profile is not shown as the program (iRIC) only started to save data at 1800 seconds (0.02 days). It goes to 9.3 days where the program failed shortly after this point. On the upstream side, the foreset moves forward as the dam becomes filled with a changing slope of the foreset as noted in the one-dimensional models. For the mean grain-size, the grain-size decreases at the front end of the foreset and remains the same in the backwater section of the dam. On the downstream side, armoring occurs initially and does not change much over time. The bed elevation has a bit of scouring and then aggradation after it. Only the initial water surface elevation is presented as the different water surface elevations did not have enough variation to merit separate lines.

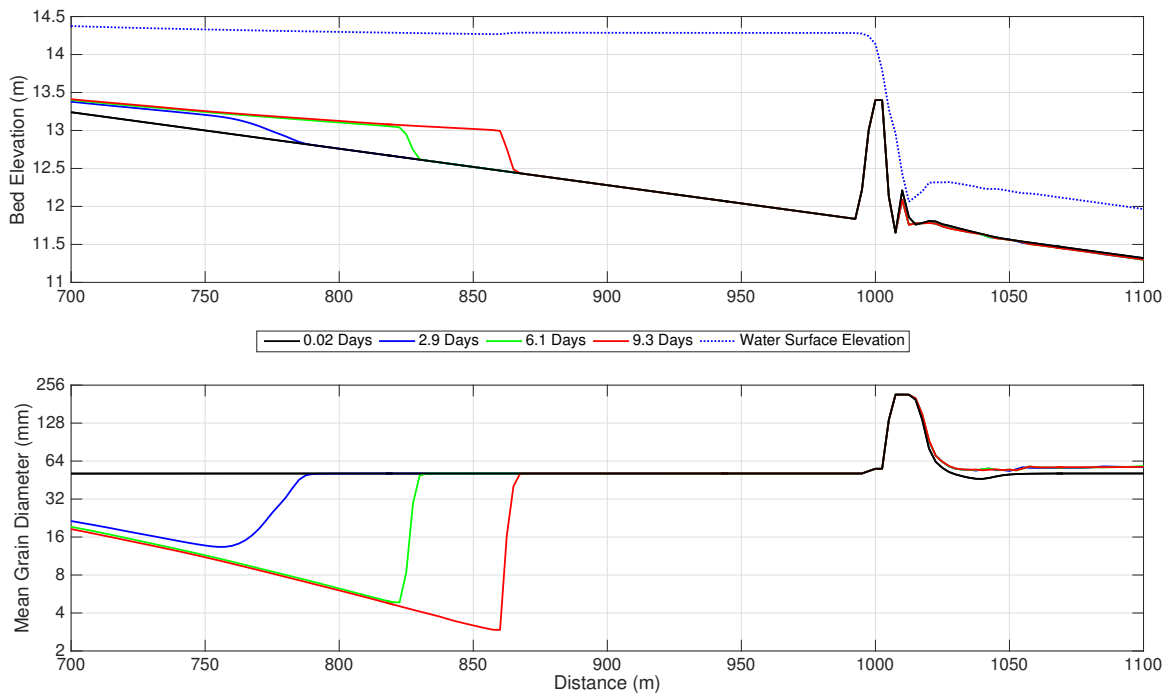


Figure 3.19: The changes over time for the bed elevation and mean grain diameter for 0.02, 2.9, 6.1 and 9.3 days for the two-dimensional model run in Nays2DH.

Chapter 4

Discussion

4.1 Flume Experiment Implications

Water surface profile

The results from the water surface profile over the dam match that of existing published literature and flow expected around dams (*Leutheusser and Birk, 1991; Leutheusser and Fan, 2001*). The water surface profile over the dam during run B is shown in Figure 3.2. At the lowest discharge, there is a clear curvature to the water surface profile as it transitions to a supercritical condition downstream of the dam. With increasing backwater conditions (e.g. run B.2), the curved water surface profile at the dam does not change substantially, but below the dam, it transitions into a subcritical flow condition, thereby producing a submerged hydraulic jump which was detected by visual inspection. Once the backwater on the downstream is made more prominent (e.g. run C.4), the curve over the dam starts to flatten and the condition is considered more submerged (*Strum, 2010*). The effect of increased downstream submergence is apparent in the highest discharge runs (series D). For the first two runs in D, the water surface is approximately constant, yet the increased submergence in Run D.3 causes the curvature over the dam to disappear and the water surface elevation behind the dam to increase, similar to what was described in the experiments of *Wu and Rajaratnam (1996)*.

Velocity profiles and measurements

The velocity profiles (Figure 3.3 show that at the dam crest, the rapid vertical transition from near-zero or negative (i.e. upstream-oriented) velocity to high-velocity a short distance above the dam suggest the shear stress at the dam crest is quite high. Once the velocity in the downstream direction along the vertical gets to the maximum value, there is a relatively large drop in the velocity which seems relatively consistent over the various runs showing the point of the fastest moving

velocity zone around the dam which could be of interest if a RoR dam has a large suspended sediment load.

Just downstream of the dam, the profile changes again so that at the bottom there is a negative velocity. This effect of velocity reversals at the downstream end of dams is well noted in reports such as *Leutheusser and Birk* (1991) and *Leutheusser and Fan* (2001), and is noted for causing the circling effect downstream of dams which can be fatal to boaters and swimmers in the river. Once the velocity in the vertical gets to around the height of the dam, the velocity increases rapidly which could imply at least some high local shear stress at this location which again might be of greater interest to suspended sediment transport. The velocity then goes to a maximum where it has a slight dip as it approaches the water surface due to shear stress from the boundary interface of the water and air.

Sediment transport connections

These results also suggest that using the shear stress from the the friction slope as currently done in the model (*Chow*, 1959), might not be the most appropriate value to use. Instead one might have to use a boundary shear stress based on a non-hydrostatic model such as in *Castro-Orgaz* (2010) and *Hager* (2010). This would help solve some of the issues with the way the current shear stress computation works but it still would not allow a 1D model to simulate upstream-oriented boundary shear stress due to the circular flow patterns, as only a 3D model would be able to accurately model these effects. If the long time duration and spatial scales afforded by the more computationally efficient 1D model is still required, however, a modeler could try to sidestep this shortcoming by restricting the ability of the model to remove sediment from the bed in the region downstream of the dam if there is a backwater effect of the dam. This has been done in a smaller extent in the model. This revelation from the flume experiment created much of the incentive to include the non-hydrostatic model for the numerical model. In the numerical model, part of the bed just downstream of the dam is set as a static bed to limit transport of sediment in that location. In addition, a new type of flow option was created downstream of the dam called "near-dam flow" which prevents flow from becoming supercritical in certain cases and transporting

too much sediment. Hence, I suggest this model represents a compromise between the accuracy potentially achievable with a multidimensional model and the computational efficiency of a 1D model.

The results as seen in Figure 3.4 show that after the calibration process, the flow in the numerical model matches the results from the flume experiment relatively well especially on the upstream end and the curvature of flow over the dam. For the higher flows, the calibration results do not match as well but for the lower flows, the water surface elevations for both of them seem to match with great agreement. In addition, one can see the curvilinear flow over the dam. The models do not capture this fully but from the runs where there was no non-hydrostatic correction and would just drop down, this matches much better. By better matching the water surface over the dam, this in turn helps to replicate the depth-averaged velocity (velocity that the model outputs) and boundary shear stress. Improved shear stress calculations should make sediment transport calculations more accurate compared to the case where no correction around the dam is performed. However, the computed sediment transport rates may remain highly uncertain, because sediment transport equations are often based on normal flow conditions (*Julien, 2010*) which means they might not be as valid for more complex flow conditions with strong velocities and stresses in the vertical direction.

The water surface profile downstream of the dam is not well captured in the model with the exception of Run A. This is partly because calibration focused more on matching the upstream end and curvature of flow. This is because, often times one dimensional models have difficulty in properly computing the water surface elevation upstream of a dam or weir (*Chaudhry, 2008; Strum, 2010*). The downstream end on the other hand is based on the proper calibration of the resistance factor used in the model. The main parameter used in calibration was changing the resistance factor and the non-hydrostatic correction values. Because a primary focus of this study was on rates and amounts of sedimentation in the reservoir upstream of a RoR dam, calibration focused on the flow over and upstream of the dam.

4.2 Controls on Sediment Storage in RoR Dam Reservoirs

Sediment supply from upstream plays a major role in determining the amount of sediment stored upstream of a RoR dam. Figures 3.6 and 3.13 show that as the sediment supply rate increases, the rate of filling also increases. Most of the time series shown in Figure 3.6, have an inflection point that indicates some sediment starts to pass over the dam while the dam is still filling up due to upstream aggradation. More aggradation happens at higher sediment supply rates due to the ideas presented by *Lane* (1955). The higher supply rates cause a steeper slope which in turn allows more sediment to become stored upstream of the dam. The higher rates also contribute to a faster time to reach equilibrium even with the additional sediment stored above the dam. There is not a linear relationship between the sediment supply rate and the sediment stored in the reservoir even though the relationship is positive. As sediment supply increases, the system appears to approach a maximum amount of sediment that can be stored above the dam.

The grain-size of the sediment supply also affects the rate and amount of sediment stored upstream of RoR dams, with finer supplied material filling the reservoir faster and to a higher level (Figures 3.6 and 3.9). However, for a constant sediment supply rate, the amount of sediment stored upstream of the dam increases with increasing grain-size (Figure 3.10). This means that as the median grain-size increase, there will be more storage available above a RoR dam. The implication of this suggests that if a dam owner wants more sedimentation capacity, a reach with a larger grain-sizes should be selected. For a finer grain-size, it would fill faster and with more sediment for a given sediment region (Figure 3.9) as sediment supply and grain-size are inherently linked. The controlling factor appears to be upstream sediment supply. Another interesting point lies in the single grain-size distribution model run that had the same median grain diameter of 28.8 mm as the base model. This one fills up much slower which might suggest that having a varied grain-size helps the dam fill faster mainly due to the lower grain-sizes present.

The height of the dam and total sediment storage are linearly related. In these simulations, however, the channel is rectangular so the volume of available storage upstream of the dam is expected to increase linearly with dam height solely due to the geometry of the system. Some

field studies have shown similar results to this in that they saw as the weir (dam) height increased, the amount of sediment behind it increased as well (*Sindelar et al.*, 2017). In the case of a more realistic river geometry, an increase in dam height would most likely cause a nonlinear increase in the stored sediment. This does however, show that dam height exhibits a relatively simple relationship to the amount of stored sediment upstream of the dam. As the dam height increases, the stored sediment above a RoR increases at a rate equal to or greater than a linear increase in the dam height.

With increasing discharge, the trend shows that as the discharge increases, the upstream region holds more sediment and it fills up quickly. Increases in discharge cause the flow depth to increase which results in high shear stresses and increased sediment transport rates so, this observation is expected. The increased sediment supply with higher discharges appears to be the main factor in causing this change. The actual flow increase appears only to be a primary factor insofar as it causes another increase in the sediment discharge rate.

4.3 Scouring of Sediment During High Flows

The unsteady flow simulations show that whether or not high flows scour sediment from the reservoir is a somewhat complex issue. For many of the unsteady models, sediment did not scour out during high flows but instead continued the trend of filling in the area behind the dam during these periods. Even when the dam was full, the excess bedload under high flows would pass over the dam and no additional sediment would be gained or lost (Figure 3.15). However, in specific cases higher flows can scour sediment from behind the dam. This does not consider the case where sediment is scoured due to a dam opening such as a sluice or weir gate which exist on some RoR dams (*Sindelar et al.*, 2017). Based on the results, it appears that RoR dams experience scouring at high flows once an equilibrium condition behind the dam occurs. Before this point, any additional sediment drops out to fill up the dam. Looking at a typical plot of the shear stress (see Figure 4.1), helps confirm this as the lower shear stress always occur just upstream of the dam. Even as the models progress, the shear stress does not increase just upstream of the dam for any of

the flow rates until sediment reaches this point and it starts to fill up. This phenomenon seems to prevent sediment from being passed for most cases before the dam reaches at least a state of quasi-equilibrium meaning that the sediment stored behind the dam is essentially unchanging. This quasi-equilibrium is not a full equilibrium as the amount of sediment above the dam does change based on the sequences of high and lower flow events (Figure 3.16).

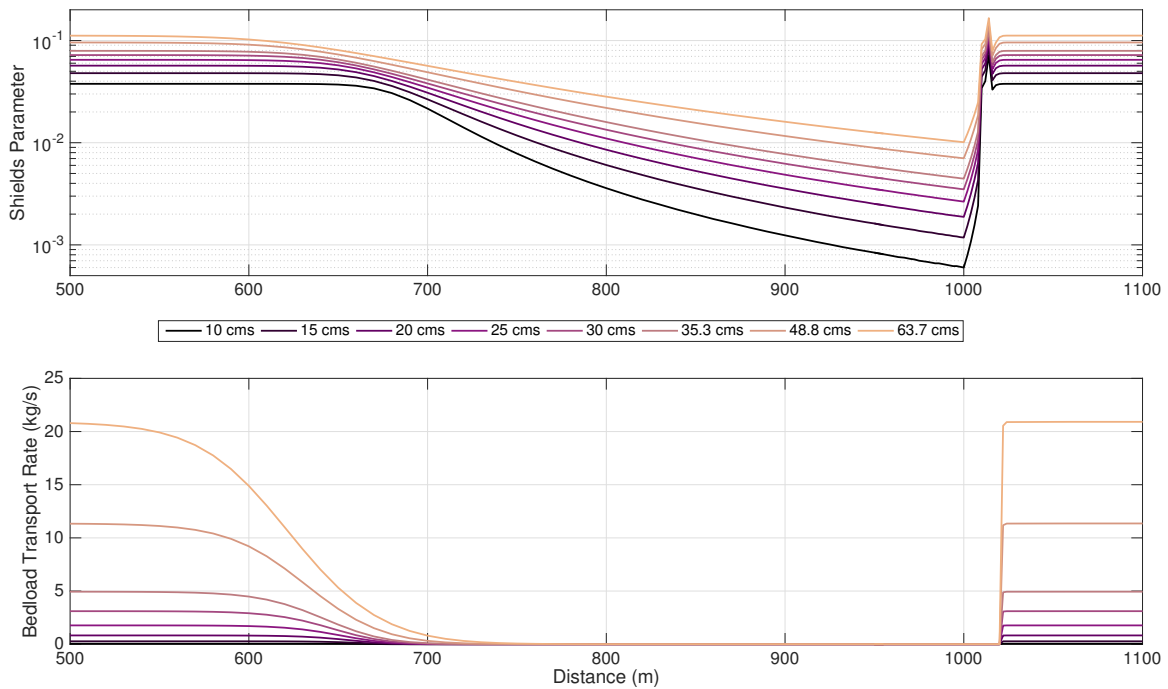


Figure 4.1: The Shields parameter and bedload transport rate over the reach for the set of runs with changes in steady discharge.

However, once the sediment in the reservoir has reached equilibrium, the numerical model shows that scouring can happen upstream of the dam during high flows. This is clearly illustrated in Figure 3.18 where the flows were increased by one cms after a day in the model time. After the equilibrium is reached at around 33 days (33 cms), the higher flows start scouring out the bed material in a way that reduces the total sediment stored behind the dam. This example is a bit contrived in that the hydrology of rivers do not behave in this manner, but it still shows a flow threshold above which increasing flows cause scour rather than aggradation in the reservoir.

Figures 3.17 and 3.16 show scouring at high flows for a more realistic hydrograph. The early periods of the simulation show the dam becoming filled with sediment without any scouring events. This occurs during high flow events in the reach as well as at flows that produce enough shear stress to move sediment. After the area behind the dam reaches a sort of dynamic equilibrium, the reach starts to go through periods of both the aggradation of sediment and then the degradation of sediment. A similar equilibrium has been described in *Sindelar et al. (2017)* where they found that the flushing efficiency of a RoR reservoir with weir gates is low when it has not reached equilibrium. In practical terms, this means that a dam operator needs a sediment equilibrium behind the dam or else sediment may not be scoured behind the dam. While this might not prove practical in certain locations as it would mean filling the dam just to allow for scouring of sediment, at specific sites, there could still be room for some water storage behind the dam. This degradation appears to require flow to be higher than a threshold of flow based on the amount of stored sediment above the dam. In this specific case, no scour occurred until the flow rate reached 21 cms. As the stored sediment in the dam increases, it appears that the threshold to pass the sediment decreases. At the highest flow events, the scouring is the greatest and causes dramatic changes. For flows greater than 35.3 cms which is the 1.1-year flow, only scouring occurs. This supports the idea that once the reservoir has reached equilibrium, low flows cause aggradation in the reservoir while periodic high flows produce scour.

The equilibrium conditions necessary for high flows to be able to produce scour in the reservoir appear to depend on the distribution of shear stresses around the dam. When the reservoir still has remaining capacity (i.e. not yet at equilibrium), the shear stresses near the dam are low enough and the transport capacity declines and deposition occurs. As more sediment is deposited in the reservoir, the shear stress increases at the downstream end, so that high flows are able to scour out sediment near the dam. Scouring under high flows also occurs when the upstream sediment supply is lower than the transport capacity of the high flow, which was the case during some of the constant supply runs presented here. Many of the models were run at equilibrium sediment supply conditions in order to preserve stability of the upstream end. See Figures 3.14 and 3.15 for the

models which shows many cases where the dam reaches a quasi-equilibrium, but there appears to be no scouring during the high flow events for most of these runs. The large flows only can move the sediment that it brings from the upstream end. Even when the dams are near capacity, the shear stresses on the downstream side are less. This means that the flow loses the transport capacity it had on the upstream end where it brings in more sediment. Further confirmation of this is seen in Figure 3.17 with the circle of points at low storage and high flows. The sediment supply in Figure 3.17 was still at an equilibrium sediment supply condition, but was limited to 1.0 kg/s during high flow events. The lack of an equilibrium sediment storage conditions means that these points with a high flow do not scour but aggrade more sediment as a way to reach this equilibrium state.

4.4 Downstream and Upstream Effects

From much of the literature on traditional dams such as *Pizzuto* (2002); *Williams and Wolman* (1985), the model produced results in line with these results and observations. On the downstream side of the dam, both armoring and incision occurred (Figure 3.8). The downstream effects of the dam appear to be consistent regardless of the sediment storage capacity of the dams during the initial (pre-equilibrium) periods when the dam traps all of the incoming sediment.

This changes once the dam either reaches a quasi-equilibrium in terms of sediment passage or the shear stresses are high enough to transport sediment. This later example is clear in Figure 3.8 with a lower dam height. This means that with less storage capacity, changes exist in how downstream areas of the dam evolve. Simulations with lower dam heights exhibit less armoring and incision downstream than simulations with higher dam heights. This impact appears to be more of temporal phenomenon as small dams or larger sediment supply rates take less time to reach the upstream equilibrium, so the period of downstream sediment deprivation is shorter. Once sediment can pass, the area downstream fills up with sediment which helps prevent further degradation and appears to then fill in the downstream scour hole at least partially. In all but a handful of cases, the increase is less than that of the original bed elevation. This appears to be as a result of the high velocities and shear stresses just downstream of the dam. Even with the replenishment of sediment

downstream of the dam, the fast moving flows are able to maintain that degradation and armoring in that location.

The effects upstream of the dam become a bit harder to quantify based on the efficacy of the dam. The actual effects upstream follow the described patterns on the upstream end of RoR dams such as in *Csiki and Rhoads (2010)* and *Pearson and Pizzuto (2015)*. This includes the development of the delta and foreset as sediment fills in the dam. Coarser sediment is further upstream while finer sediment is able to move downstream further into the backwater area of the dam. In all the models, this trend occurred which can be best seen in Figure 3.5 with the layers of stratigraphy upstream of the dam on the foreset. Scenarios with a greater storage efficacy, such as those with a taller dam height, have more extreme changes to the upstream bed elevation. Dams that can reach equilibrium faster, such as shorter dams, can have minor impacts to the upstream end. For example, Figure 3.11 shows that short dams, store relatively little sediment, and downstream of shorter dams (as represented by the dotted lines closest to the right side in Figure 3.8), there are some initial changes, but the bed elevation returns to pre-dam levels relatively quickly. The median grain-size downstream of shorter dams still increases, but it does not increase to the extent that happens for dams with less upstream storage. This also gives rise to the idea that the upstream and downstream parts of the dams have connected effects based on the storage efficacy. As the amount of available storage on the upstream increase, more sediment is stored upstream which means that the downstream will have greater impacts when looking at a long time scale to the point of where sediment can be passed over the dam.

Both these downstream and upstream effects of the RoR dam on the river morphology have important implications related to the both the longer term geomorphology as well as aquatic habitat. While the sediment is not being passed over the dam, the sediment starved downstream can impact far downstream. This might cause reaches further down to degrade further which might negatively impact infrastructure such as other RoR dam and bridges. Aquatic habitat such as certain species of salmon need specific grain-sizes of sediment to spawn (*Fuller et al., 2016*). The impacts of

these dams were well studied as part of this research, yet the compounding nature of these were not fully captured.

4.5 Two Dimensional Model

The results of the two dimensional model did not provide many additional insights into the workings of a 1D model. On the upstream side, the foreset developed as in the one-dimensional model with initially lower grain-sizes as it develops and the reservoir fills up. On the downstream side, both the degradation and armoring of the bed material occurred as predicted in the 1D model. The biggest difference between the models was that the 2D model predicted the development of a pile of sediment just downstream of the scour hole. It was not clear if this is a modeling artifact or a potentially real response. Some field observations have shown that bars develop downstream of many RoR dams (*Csiki and Rhoads, 2014*) which could be similar to what has developed here. Due to the lack of major differences (and thus lack of new information) and much longer run time of these models, more models were not run. It was hard to directly compare the results of the 1D and 2D model runs as they used a different sediment transport relationship. The 1D model uses the Wilcock and Crowe method (*Wilcock and Crowe, 2003*) while the 2D model uses the Ashida-Michue (1972) relationship for mixed-grain-sizes (*Nelson et al., 2016*). Different sediment transport relationships can yield vastly different results due to the difference in each of these models. In addition, the handful of models that were run such as the results seen in Figure 3.19 had many issues with finishing the run. The iRIC software with Nays2DH would often crash before completion with a run time of over a week. This suggested that the application of RoR dams with this model especially at this time and spatial scale might not be the most appropriate.

Two dimensional models might be useful in a more specific case of a RoR dam. For this general case, 2D models were not very informative because issues such as bar development, varying width channels and ability to evacuate sediment by weir gates were not considered. However, higher dimensional models might prove useful in better understanding the sediment dynamics around RoR dams. The flume experiments showed complex flow patterns around the dam that did not exhibit

the behavior of the depth-averaged velocity used in both the 1D and 2D models. In addition, the results showed vertical velocity components which cannot be represented in depth-averaged flow calculations. The move to a 3D model that does not employ the hydrostatic and depth-averaged velocity assumptions could help improve the results. For example, some field observations (*Pearson and Pizzuto, 2015*) have shown the formation of sediment ramps as a method of sediment transport. The circular nature of flow just upstream of the dam might suggest that this could be the case in the flume experiment. Using a detailed 3D model in this zone could help verify this observation to better understand sediment transport over a RoR dam. Other studies have found this circular flow vortex pattern behind a dam (*Csiki and Rhoads, 2010*) which help give rise to the need for a more complex flow model upstream of these dams.

Chapter 5

Conclusion

This study used a one-dimensional morphodynamic model, validated and improved by both a flume experiment and a two-dimensional model, to better understand how Run-of-River dams impact the upstream and downstream areas of a river. Due to the small size of these dams, they often are assumed to have a no impact or negligible impact to the river morphology. While evidence for this is not well documented, some studies such as *Csiki and Rhoads (2014)* have shown this to be the case. In this study, we showed that these dams can have substantial impacts on the river in terms of aggradation and degradation of the bed material as well as changes to the grain-size distribution and median grain-size. In addition, these dams appear to impact sediment transport in a way as to merit the research of the impact these have on the stream as in many cases (but not always) the dam deprived the downstream section of any sediment suggesting cascading impacts further downstream. Much of the upstream impacts on morphology was controlled by the sediment supply rate, with higher supplies causing greater volumes of reservoir sedimentation. Downstream impacts were largely controlled by the amount of time it takes to fill the reservoir upstream of the dam, because during this time the downstream reach is starved of sediment, so simulations with smaller dams, higher sediment supplies, and finer grain-sizes (which all fill faster) had lesser downstream impacts. Overall, these morphological changes could have broader implications such as various ecological concerns such as the need for certain types of fish to have a specific grain-size to be able to reproduce (*Fuller et al., 2016*).

This study also identified a mechanism for scouring sediment from RoR reservoirs during high flow events while lower flows fill up the region behind the dam. This way help explain the lack of expected sediment behind many RoR dams such as those in *Csiki and Rhoads (2014)*; *Pearson and Pizzuto (2015)* and suggest that a RoR dam (without a weir or sluice gate) could be constructed or designed in such a way that allows a starting equilibrium condition. With the connection of this model to the iRIC interface, anyone can use this model to investigate a specific site or investigate

various scenarios such as changing dam height, flow rates and sediment supply rate around the dam. While it can be difficult to quantify the management implications at a RoR dam site without the specific conditions, this study helped to provide a clearer framework in this regards.

The one-dimensional model used in this study allows for many runs over long time and spatial scales. Yet, it does not capture everything present around the dam due to both the rapidly varied and non-hydrostatic flow around the dam that might cause changes to sediment transport in the model. In my model, part of this was resolved a bit with the addition of a correction term into the hydraulic computations, yet this does not capture everything. To solve this problem, one must abandon the hydrostatic assumption which would imply a 3D morphodynamic model that allows for differences in velocities over a vertical water column is needed. This would capture the circular flow conditions around the dam as described in the flume experiment as a way to better see the shear stresses impacting the sediment transport rates in this area. In addition, one could help resolve this problem through the use of a mobile bed flume experiment with a RoR dam that would allow researchers to better control for variables such as sediment supply rate, flow rate and grain-size distribution. A flume experiment could then be used to inform a more detailed 3D model to better understand the mechanisms of sediment transport around RoR dams and their impacts on channel morphology. More long term observations of RoR dams would also prove useful before and after large flood events.

Bibliography

- Anderson, D., H. Moggridge, P. Warren, and J. Shucksmith (2015), The impacts of ‘run-of-river’ hydropower on the physical and ecological condition of rivers, *Water and Environment Journal*, 29(2), 268–276, doi:10.1111/wej.12101.
- Bhallamudi, S. M., and M. H. Chaudhry (1991), Numerical modeling of aggradation and degradation in alluvial channels, *Journal of Hydraulic Engineering*, 117(9), 1145–1164, doi:10.1061/(ASCE)0733-9429(1991)117:9(1145).
- Castro-Orgaz, O. (2010), Steady open channel flows with curved streamlines: the Fawer approach revised, *Environmental Fluid Mechanics*, 10(3), 297–310, doi:10.1007/s10652-009-9157-0.
- Chaudhry, M. H. (2008), *Open-Channel Flow*, Springer, New York, NY.
- Chow, V. T. (1959), *Open Channel-Hydraulics*, McGraw-Hill Book Company, New York City.
- Csiki, S., and B. L. Rhoads (2010), Hydraulic and geomorphological effects of run-of-river dams, *Progress in Physical Geography*, 34(6), 755–780.
- Csiki, S. J., and B. L. Rhoads (2014), Influence of four run-of-river dams on channel morphology and sediment characteristics in Illinois, USA, *Geomorphology*, 206, 215 – 229, doi:<https://doi.org/10.1016/j.geomorph.2013.10.009>.
- Dietrich, W. E. (1982), Settling velocity of natural particles, *Water Resources Research*, 18(6), 1615–1626, doi:10.1029/WR018i006p01615.
- Fuller, T. K., J. G. Venditti, P. A. Nelson, and W. J. Palen (2016), Modeling grain size adjustments in the downstream reach following run-of-river development, *Water Resources Research*, 52(4), 2770–2788, doi:10.1002/2015WR017992.
- Garcia, M., and G. Parker (1991), Entrainment of bed sediment into suspension, *Journal of Hydraulic Engineering*, 117(4), 414–435.

- Goring, D. G., and V. I. Nikora (2002), Despiking acoustic doppler velocimeter data, *Journal of Hydraulic Engineering*, 128(1), 117–126, doi:10.1061/(ASCE)0733-9429(2002)128:1(117).
- Hager, W. H. (2010), Comments on “Steady open channel flows with curved streamlines: The Fawer approach revised”, *Environmental Fluid Mechanics*, 10(4), 491–494, doi:10.1007/s10652-010-9178-8.
- Henderson, F. M. (1966), *Open Channel Flow*, Macmillan Publishing Co, Inc., New York City.
- Hirano, M. (1971), River bed degradation with armouring, *Transactions of the Japan Society of Civil Engineers*, 3, 194–195.
- Jayjack, N. (2018), Hydropower regulatory efficiency act of 2013, <https://www.ferc.gov/industries/hydropower/indus-act/efficiency-act.asp>, [Online; accessed 22-May-2018].
- Julien, P. Y. (2010), *Erosion and Sedimentation*, Cambridge University Press, Cambridge, UK.
- Lajczak, A. (1996), Modelling the long-term course of non-flushed reservoir sedimentation and estimating the life of dams, *Earth Surface Processes and Landforms*, 21(12), 1091–1107, doi:10.1002/(SICI)1096-9837(199612)21:12<1091::AID-ESP653>3.0.CO;2-2.
- Lane, E. W. (1955), The importance of fluvial morphology in hydraulic engineering, *Proceedings of the American Society of Civil Engineers*, 81, 745.
- Leutheusser, H. J., and W. M. Birk (1991), Drownproofing of low overflow structures, *Journal of Hydraulic Engineering*, 117(2), 205–213, doi:10.1061/(ASCE)0733-9429(1991)117:2(205).
- Leutheusser, H. J., and J. J. Fan (2001), Backward flow velocities of submerged hydraulic jumps, *Journal of Hydraulic Engineering*, 127(6), 514–517, doi:10.1061/(ASCE)0733-9429(2001)127:6(514).
- Lohrmann, A., R. Cabrera, and N. Kraus (1994), Acoustic-doppler velocimeter (ADV) for laboratory use, *Fundamentals and Advancements in Hydraulic Measurements and Experiments*, pp. 351–365.

- McDonald, R., J. Nelson, V. Paragamian, and G. Barton (2010), Modeling the effect of flow and sediment transport on white sturgeon spawning habitat in the Kootenai River, Idaho, *Journal of Hydraulic Engineering*, 136(12), 1077–1092, doi:10.1061/(ASCE)HY.1943-7900.0000283.
- Morgan, J. A., and P. A. Nelson (2016), One-dimensional modeling of sediment pulse dynamics, Unpublished manuscript to Water Resources Research.
- Nelson, J. M., Y. Shimizu, T. Abe, K. Asahi, M. Gamou, T. Inoue, T. Iwasaki, T. Kakinuma, S. Kawamura, I. Kimura, T. Kyuka, R. R. McDonald, M. Nabi, M. Nakatsugawa, F. R. Simoes, H. Takebayashi, and Y. Watanabe (2016), The international River Interface Cooperative: Public domain flow and morphodynamics software for education and applications, *Advances in Water Resources*, 93, 62 – 74, doi:https://doi.org/10.1016/j.advwatres.2015.09.017.
- Nikora, V. I., and D. G. Goring (1998), ADV measurements of turbulence: Can we improve their interpretation?, *Journal of Hydraulic Engineering*, 124(6), 630–634, doi:10.1061/(ASCE)0733-9429(1998)124:6(630).
- Nortek (2015), *Comprehensive Manual for Nortek Products*, Nortek As.
- Parker, G. (1991), Selective sorting and abrasion of river gravel. II: Applications, *Journal of Hydraulic Engineering*, 117(2), 150–171, doi:10.1061/(ASCE)0733-9429(1991)117:2(150).
- Parker, G. (2006), *1D Sediment Transport Morphodynamics with Applications to Rivers and Turbidity Currents*, E-Book, University of Illinois.
- Pearson, A. J., and J. Pizzuto (2015), Bedload transport over run-of-river dams, Delaware, U.S.A., *Geomorphology*, 248, 382 – 395, doi:https://doi.org/10.1016/j.geomorph.2015.07.025.
- Pizzuto, J. (2002), Effects of dam removal on river form and process, *BioScience*, 52(8), 683, doi:10.1641/0006-3568(2002)052[0683:EODROR]2.0.CO;2.

- Sindelar, C., J. Schobesberger, and H. Habersack (2017), Effects of weir height and reservoir widening on sediment continuity at run-of-river hydropower plants in gravel bed rivers, *Geomorphology*, 291(Supplement C), 106 – 115, doi:<https://doi.org/10.1016/j.geomorph.2016.07.007>.
- Strum, T. W. (2010), *Open Channel Hydraulics*, McGraw-Hill Higher Education, New York, NY.
- USGS (2018), National water information system data available on the world wide web (USGS water data for the nation), doi:<http://dx.doi.org/10.5066/F7P55KJN>.
- Viparelli, E., O. E. Sequeiros, A. Cantelli, P. R. Wilcock, and G. Parker (2010a), River morphodynamics with creation/consumption of grain size stratigraphy 2: numerical model, *Journal of Hydraulic Research*, 48(6), 727–741, doi:10.1080/00221686.2010.526759.
- Viparelli, E., R. Haydel, M. Salvaro, P. R. Wilcock, and G. Parker (2010b), River morphodynamics with creation/consumption of grain size stratigraphy 1: laboratory experiments, *Journal of Hydraulic Research*, 48(6), 715–726, doi:10.1080/00221686.2010.515383.
- Warren, G. S. (2014), Hydropower: Time for a small makeover emerging challenges to good governance in the great lakes: Comparative models, *Indiana International & Comparative Law Review*, 24.
- Wilcock, P. R., and J. C. Crowe (2003), Surface-based transport model for mixed-size sediment, *Journal of Hydraulic Engineering*, 129(2), 120–128, doi:10.1061/(ASCE)0733-9429(2003)129:2(120).
- Williams, G. P., and M. G. Wolman (1985), Downstream effects of dams on alluvial rivers, *U.S. Geological Survey, Prof. Pap.; (United States)*, 1286.
- Wright, S., and G. Parker (2004), Flow resistance and suspended load in sand-bed rivers: simplified stratification model, *Journal of Hydraulic Engineering*, 130(8), 796–805.

Wu, S., and N. Rajaratnam (1996), Submerged flow regimes of rectangular sharp-crested weirs, *Journal of Hydraulic Engineering*, 122(7), 412–414, doi:10.1061/(ASCE)0733-9429(1996)122:7(412).

Appendix A

iRIC Interface Guide

A.1 Introduction

This document explains how to use and successfully run the one-dimensional morphodynamic with stratigraphy model created for use in the iRIC (International River Interface Cooperative, *i-ric.org*) environment. For information on the fundamentals behind the model and the various computations used, see the methods section of the accompanying document.

A.2 Guide

This section creates a guide on how to use the model including the initial set-up.

1. Connect the model with iRIC

- (a) Extract from the *ID_morpho.zip* zip file and place the folder in the *solvers* folder where iRIC is installed on the local machine. It should be in there in a similar manner to the other solvers in there. In this folder there is the .exe file that runs the program, the .xml file that tells iRIC what to do, various other inputs and various .dll files that contain necessary libraries for the program to run.
- (b) Open iRIC and select a new project. If the extracted zip file was placed in there correctly, it will show up under the various solvers one can pick from. Select this solver to use for the rest of the guide.

2. Set-up the model

- (a) Save a new project.
- (b) Set up the grid conditions using the simple grid model. This model only preforms calculations on a rectangular channel right now so the number of nodes in the cross

stream direction doesn't matter. It can do calculations on variable width channels too. A curved channel will work, but it doesn't changed the overall model results. The main parameters to change are the slope, the number of downstream nodes and any other elevation parameters as necessary.

- (c) Adjust the grid elevation manual using the tools in the editing page. This can include adjusting the elevation in certain locations such as creating a dam location. Also, one can define the location of obstacles for cells (locations where the ground can't be eroded and computes non-hydrostatic flow) and near dam flow locations (computes non-hydrostatic flow and some other adjustments).

3. Adjust parameters in the calculation conditions

- (a) In the **Boundary Conditions** tab, fill out the parameters. The time step should be short enough so that there are no model instabilities. *User Supplied Qs* means that the user picks a volumetric sediment supply rate to use on the upstream end. *Equilibrium Supply Rate* means that the program computes the upstream supply rate based on the rate from the sediment transport equations as a way to maintain equilibrium. In this later case, the sediment supply rate should be set at zero. For the downstream boundary conditions, select the appropriate one for the model. The downstream water surface elevation only needs to be set in the case of when *Fixed Water Surface Elevation*.
- (b) In the **Sediment Transport** tab, select values for each parameter. For the bedload equations see the document for the differences between the models. The layer thickness should be thicker than the roughness height times the d_{90} of the bed material or else problems could occur. When setting the grain-size distribution data, make sure the grain-size has the same values and same number of rows in each case and that it is in ascending order.

- (c) In the **Dam Information** tab, set the dam height and if non-hydrostatic flow is to be used for the model. See the document for information on how the non-hydrostatic flow is computed.
- (d) In the **File Saving** tab first set the run name in two digit integer. Set the time of output for both the simplified .csv file and the normal output time that outputs a detailed .csv file and the iRIC information. For the file saving location, selected an existing file location to save the data (include the slash at the end). **IMPORTANT** - In this data location, create two new files. The first file name is just the two digit integer and the other is 'simp' plus the two digit integer. For example, if the integer is 3, the first file is named *03* and the second file is named *simp03*. Also, if the integer is 64, the first file is named *64* and the second file is named *simp64*
- (e) In the **Numerical Constants** tab set the various constants used in the model. These all have appropriate default values and do not have to be changed.

4. Run the model.

- (a) The model will display the output time and when it saves the various files.
- (b) The model might crash if errors occur. These could be from a variety of errors and may be from errors in the iRIC software or the underlying model code.

5. Display the model results.

- (a) The model outputs the following in iRIC:
 - i. Water Surface Elevation (m)
 - ii. Bed Elevation (m)
 - iii. Velocity (m/s)
 - iv. Shear Stress (Pa)
 - v. Shields Stress
 - vi. D_{16} (mm) of bed

vii. D_{50} (mm) of bed

viii. D_{84} (mm) of bed

ix. Q_s (kg/s)

- (b) The model also outputs two different file types of the important parameters that were computed in .csv files so that one can display the data in other formats as wanted.

A.3 Conclusion

This guide provides a way to make sure the one-dimensional morphodynamic model with stratigraphy runs properly within the iRIC environment. For a more technical view on the fundamentals behind the model see the methods sections of the main document.

A.4 Attached Files

Attached is the *ID_morpho.zip* that contains the necessary files to run this program in the iRIC environment.

Appendix B

Suspended Sediment Transport

Suspended sediment transport calculations in the model are based on *Garcia and Parker (1991)* and *Wright and Parker (2004)* with a modification for gravel rivers.

The suspended sediment model requires the grain-size distribution (and related parameters), the hydraulic parameters such as shear stress and depth of flow and the basic elevation data of the surface. For each grain-size in the surface distribution, the following parameters are found.

First, the particle Reynolds number, Re_p is found by:

$$Re_p = \frac{\sqrt{Rgd_s}d_s}{\nu} \quad (\text{B.1})$$

where R is the submerged specific gravity of the sediment (1.65), g is the acceleration due to gravity, d_s is the grain-size and ν is the kinematic viscosity of water. Next, the fall velocity, ω of each sediment size is found based on the relationship by *Dietrich (1982)*. In order to account for large particles, a function of the Reynolds particle number, $f(Re_p)$ is found. If $Re_p \leq 233.7$, then $f(Re_p) = Re_p^{0.6}$ and otherwise $f(Re_p) = 26.38$. This value is used in a parameter, X to find the the entrainment rate, E_s . If the ratio of the shear velocity, u_* (function of hydraulic calculations) to the the fall velocity is greater than 0.4 then:

$$X = \frac{u_*}{\omega} f(Re_p) S_0^{0.08} \left(\frac{d_s}{d_{50}} \right)^{0.2} \quad (\text{B.2})$$

where S_0 is the bed slope and d_{50} is the median grain diameter of the surface grains. Otherwise if $u_*/\omega \leq 0.4$, then $X = 0$. From this, the entrainment rate can be found by:

$$E_s = \frac{B(\lambda X)^5}{1 + \frac{B}{0.3}(\lambda X)^5} \quad (\text{B.3})$$

where B is a constant equal to $7.8E - 7$ and $\lambda = 1 - 0.298\sigma$ and is constant for each grain-size distribution as σ is the geometric standard deviation for a grain-size distribution. The concentration at five percent the depth, C_5 is:

$$C_5 = E_s F_b \quad (\text{B.4})$$

where F_b is the percentage of sediment at that specific class (pdf of grain-size distribution). Once these calculations are complete for all grain-sizes, the concentration is summed to find the total concentration at five percent the total depth (C_{5t}). Next, a correction value, α is found. If $C_{5t}/S_0 \leq 10$ then:

$$\alpha = 1 - 0.06 \left(\frac{C_{5t}}{S_0} \right)^{0.77} \quad (\text{B.5})$$

Otherwise:

$$\alpha = 0.67 - 0.0025 \left(\frac{C_{5t}}{S_0} \right) \quad (\text{B.6})$$

In addition, the smallest value that α can be was set to $\alpha = 0.5$ based on the range of data used in the formulation of this correction factor. Next, a parameter, Z_r is found using:

$$Z_r = \frac{\omega}{\alpha \kappa u_*} \quad (\text{B.7})$$

where $\kappa = 0.4$ and is the von Karman's constant. The suspended sediment transport per unit width for each grain-size is then found by:

$$q_{si} = \frac{u_* E_s H I F_b}{\kappa} \quad (\text{B.8})$$

where I is an integral based on the the velocity profile and the concentration profile of the flow and sediment in the water. If assuming both of these follow logarithmic profile, this integral is only a function of Z_r . An approximation of this integral, I is as follows if $Z_r \leq 1$:

$$I \approx 0.679 \exp(-2.23Z_r) \quad (\text{B.9})$$

otherwise:

$$I \approx 0.073Z_r^{-1.44} \quad (\text{B.10})$$

Once the suspended sediment transport rate is found for each grain-size, it summed up to find the total suspended sediment transport rate at each spatial node. The new distribution of grain-sizes in the suspended sediment load can then be determined. This information can then be used in the Exner equation to update the bed elevation.